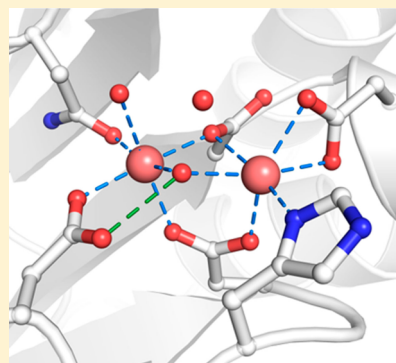


Formiminoglutamase from *Trypanosoma Cruzi* Is An Arginase-Like Manganese Metalloenzyme

Yang Hai, Reilly Jane Dugery,[†] David Healy, and David W. Christianson*

Roy and Diana Vagelos Laboratories, Department of Chemistry, University of Pennsylvania, Philadelphia, PA 19104-6323, U.S.A.

ABSTRACT: The crystal structure of formiminoglutamase from *Trypanosoma cruzi* (TcFIGase) is reported at 1.85 Å resolution. Although the structure of this enzyme was previously determined by the Structural Genomics of Pathogenic Protozoa Consortium (PDB accession code 2A0M), this structure was determined at low pH and lacked bound metal ions; accordingly, the protein was simply annotated as “arginase superfamily protein” with undetermined function. We show that reconstitution of this protein with Mn^{2+} confers maximal catalytic activity in the hydrolysis of formiminoglutamate to yield glutamate and formamide, thereby demonstrating that this protein is a metal-dependent formiminoglutamase. Equilibration of TcFIGase crystals with $MnCl_2$ at higher pH yields a binuclear manganese cluster similar to that observed in arginase, except that the histidine ligand to the Mn^{2+}_A ion of arginase is an asparagine ligand (N114) to the Mn^{2+}_A ion of TcFIGase. The crystal structure of N114H TcFIGase reveals a binuclear manganese cluster essentially identical to that of arginase, but the mutant exhibits a modest 35% loss of catalytic efficiency (k_{cat}/K_M). Interestingly, when TcFIGase is prepared and crystallized in the absence of reducing agents at low pH, a disulfide linkage forms between C35 and C242 in the active site. When reconstituted with Mn^{2+} at higher pH, this oxidized enzyme exhibits a modest 33% loss of catalytic efficiency. Structure determinations of the metal-free and metal-bound forms of oxidized TcFIGase reveal that although disulfide formation constricts the main entrance to the active site, other structural changes open alternative channels to the active site that may help sustain catalytic activity.



INTRODUCTION

L-Histidine catabolism in prokaryotes and eukaryotes is achieved through one of six histidine utilization pathways, as currently outlined in the MetaCyc database.¹ These pathways are classified by the enzyme that catalyzes the first step, which is either a histidase (pathways I–III and VI) or a transaminase (pathways IV and V).² In the transaminase pathways, L-histidine is converted into imidazolylpyruvate by either histidine-2-oxoglutarate aminotransferase in prokaryotes (pathway IV),³ or histidine-pyruvate aminotransferase in eukaryotes (pathway V),⁴ which is then reduced to imidazolylactate.⁵ In the histidase pathways, L-histidine is converted into urocanic acid and ammonia.^{6,7} Pathways I–III then proceed in a similar manner through the key intermediate N-formimino-L-glutamate (also known as L-formiminoglutamic acid), which is subsequently degraded to form L-glutamate by a different enzyme in each pathway (Figure 1). Pathway III is mainly found in mammals,⁸ whereas pathways I and II are widely conserved in bacteria and operated by the *hut* gene.⁹ In pathway VI, 4-imidazolone-5-propionate, the intermediate shared with pathway I–III, is enzymatically oxidized into L-hydantoin-5-propionate,^{10,11} which is further processed in some bacteria by hydrolysis to form N-carbamyl-L-glutamate and thence L-glutamate.¹²

Formiminoglutamase (FIGase, also known as N-formimino-L-glutamate formiminohydrolase), catalyzes the final step in histidine utilization pathway I by catalyzing the hydrolysis of the imino group of N-formimino-L-glutamate to form L-glutamate and formamide (Figure 1). Formiminoglutamase

belongs to the metal-dependent arginase/ureohydrolase superfamily, which also includes proclavaminic acid amidinohydrolase, agmatinase, guanidinobutyrase, and guanidinopropionase.^{13,14} The first member of this enzyme family to yield a crystal structure was rat arginase I,¹⁵ which revealed a unique α/β fold and a binuclear manganese cluster required for catalysis. Subsequently determined crystal structures of other members of this family revealed similar tertiary structures and conservation of the catalytically obligatory binuclear manganese cluster.^{16–19}

Two formiminoglutamase crystal structures have been determined by structural genomics consortia and are currently available in the Protein Data Bank (www.rcsb.org). Surprisingly, however, neither of these structures appears to be that of a functional metalloenzyme. The structure of formiminoglutamase from *Vibrio cholerae* (PDB entry 1XFK) does not contain bound metal ions, and the structure of formiminoglutamase from *Bacillus subtilis* (PDB entry 3M1R) contains a binuclear calcium cluster instead of the binuclear manganese cluster expected for members of the arginase/ureohydrolase family. Additionally, the crystal structure of a protein of undetermined function annotated as “arginase superfamily protein” from *Trypanosoma cruzi* was determined by the Structural Genomics of Pathogenic Protozoa Consortium²⁰ (PDB entry 2A0M), but this protein does not contain bound metal ions. However, given that (1) this protein

Received: October 1, 2013

Revised: November 8, 2013

Published: November 21, 2013



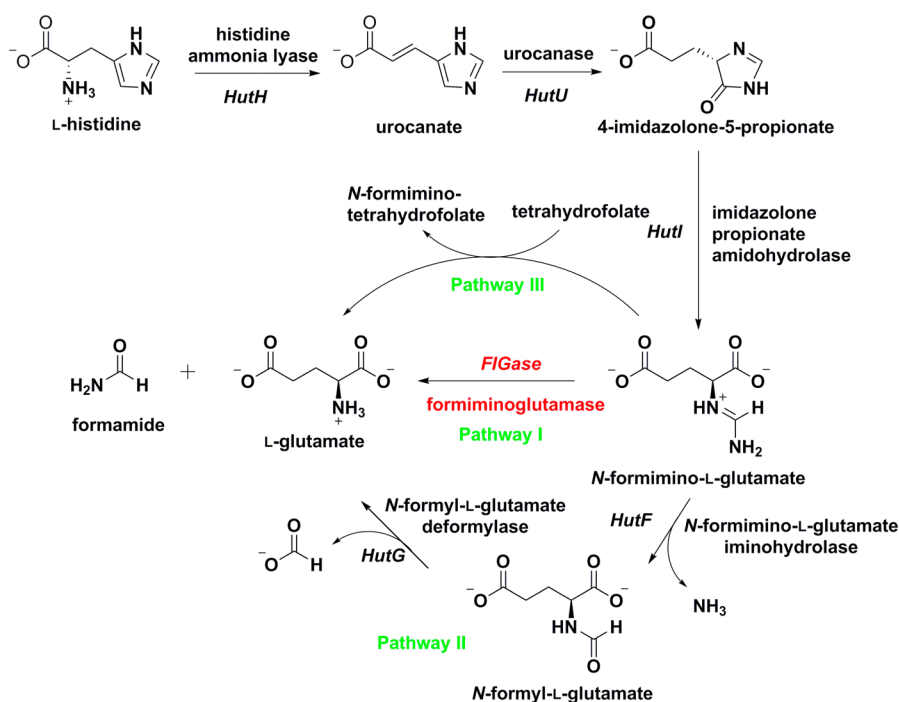


Figure 1. Pathways I–III for L-histidine catabolism. Formiminoglutamase catalyzes the final step in histidine utilization pathway I.

adopts the classic α/β arginase fold, (2) this protein exhibits 24% sequence identity with formiminoglutamase from *B. subtilis*, and (3) this protein contains conserved residues for Mn^{2+} coordination, we hypothesized that this protein is in fact *T. cruzi* formiminoglutamase (TcFIGase) crystallized in its metal-free state at pH 4.0. It should be noted that although atomic coordinates for these formiminoglutamase crystal structures are available in the Protein Data Bank, formal research papers describing the structure determinations have not been published.

Intriguingly, while members of the arginase/ureohydrolase family typically contain two conserved histidine and four conserved aspartate ligands to the binuclear manganese cluster, one of the histidine ligands is substituted by an asparagine ligand in formiminoglutamase from *B. subtilis* and TcFIGase. Although it might not be clear from the available crystal structures whether formiminoglutamases are actually Ca^{2+} -dependent enzymes, or whether they are metalloenzymes at all, formiminoglutamases from *Aerobacter aerogenes* and *B. subtilis* exhibit maximal activity in the presence of Mn^{2+} .^{21,22} Thus, despite the substitution of the putative metal ligand in TcFIGase, we hypothesized that it, too, is a manganese metalloenzyme.

Here, we demonstrate that TcFIGase exhibits maximal catalytic activity in the presence of Mn^{2+} , thereby confirming that it is a manganese metalloenzyme, and we report the crystal structure of TcFIGase containing an intact binuclear manganese cluster. We also report the crystal structure of N114H TcFIGase, in which the mutation restores a histidine Mn^{2+} ligand as found in arginase and related ureohydrolases. On the basis of comparisons between TcFIGase and arginase, we propose a catalytic mechanism for the hydrolysis of formiminoglutamate. Finally, we report the crystal structure of TcFIGase in its oxidized form (TcFIGase_{ox}), bearing a disulfide linkage between active site residues C35 and C242, and we show that TcFIGase_{ox} exhibits nearly full catalytic activity despite structural changes triggered in the active site by disulfide bond formation.

MATERIALS AND METHODS

Materials. Dipicolinic acid, manganese(II) chloride tetrahydrate ($\geq 99\%$), cobalt chloride hexahydrate ($>99\%$), nickel chloride hexahydrate, L-arginine, α -isonitrosopropiophenone, 3-guanidinopropionic acid, 4-guanidinobutyric acid, agmatine sulfate salt, L-2-amino-3-guanidinopropionic acid hydrochloride, N_α -acetyl-L-arginine, L-homoarginine hydrochloride, potassium ferricyanide and sodium nitroprusside dihydrate were purchased from Sigma. Magnesium chloride hexahydrate (99%) was purchased from Acros Organics. Tris(2-carboxyethyl)phosphine hydrochloride (98%, TCEP) was purchased from Gold Biotechnology. α -Guanidinoglutamic acid was purchased from Cayman Chemical. A 50% (w/v) PEG 3350 solution, 100% PEG 300 solution, and 3.4 M sodium malonate solution were purchased from Hampton Research. Chelex 100 resin (molecular biology grade) was purchased from Bio-Rad. L-Formiminoglutamic acid was purchased from Dalton Pharma Services (Canada). Ethylenediaminetetraacetic acid tetrasodium salt (99.5%), zinc chloride (99.1%), ferrous chloride tetrahydrate, and all other chemicals were purchased from Fisher Scientific.

Mutagenesis, Expression, and Purification of TcFIGase.

The pET plasmid encoding wild-type *T. cruzi* formiminoglutamase (TcFIGase) with an N-terminal His₆-tag was kindly provided by Dr. Ethan Merritt of the Structural Genomics of Pathogenic Protozoa Consortium at the University of Washington. Four mutants were generated using the QuickChange method (Stratagene) with the wild-type gene as template and the following primers (underlined bases indicate mutated codons): N114H, 5'-CCT TTT GTG ATT GGC GGA GGA CAC GAC CAG TCG GC-3' (sense), 5'-GCC GAC TGG TCG TGT CCT CCG CCA ATC ACA AAA GG-3' (antisense); R144K, 5'-GGA TGT TAA ACC ACC TCT GTC GG-3' (sense), 5'-CCG ACA GAG GTG GTT TAA CAT CC-3' (antisense); R144E, 5'-GGA TGT TGA ACC ACC TCT GTC GG-3' (sense), 5'-CCG ACA GAG GTG GTT CAA CAT CC-3' (antisense); R144A, 5'-CTC ATT TGG ATG TTG CCC CAC CTC TGT CGG-3' (sense),

Table 1. Data Collection and Refinement Statistics

enzyme structure	Mn ²⁺ ₂ -TcFIGase (pH 8.0)	Mn ²⁺ ₂ -N114H TcFIGase (pH 7.5)	Apo-TcFIGase _{ox} (pH 4.6)	Mn ²⁺ ₂ -TcFIGase _{ox} (pH 6.0)	Mn ²⁺ ₂ -TcFIGase _{ox} (pH 8.5)
A. data collection					
wavelength (Å)	1.5418	1.075	1.075	1.5418	1.5418
resolution limits (Å)	50.0–1.85	50.0–1.80	50.0–1.53	50.0–1.80	50.0–1.52
no. total/unique reflections	108650/44906	156011/24658	187951/40029	77546/24341	144418/40463
space group	H3	H3	H3	H3	H3
a, b, c (Å)	128.9, 128.9, 85.4	129.4, 129.4, 42.5	129.4, 129.4, 42.6	129.5, 129.5, 42.7	129.7, 129.7, 42.5
α, β, γ (deg)	90, 90, 120	90, 90, 120	90, 90, 120	90, 90, 120	90, 90, 120
completeness ^a (%)	99.2 (98.8)	100 (100)	99.9 (100)	98.2 (97.3)	98.4 (95.1)
I/σ _I ^a	14.2 (2.0)	19.0 (2.9)	17.3 (2.7)	10.0 (2.3)	14.4 (2.7)
R _{sym} ^{a,b}	0.059 (0.438)	0.088 (0.754)	0.077 (0.527)	0.117 (0.466)	0.077 (0.422)
redundancy ^a	2.5 (2.4)	6.3 (6.1)	4.7 (4.5)	3.2 (3.1)	3.6 (3.2)
B. refinement					
no. of reflections used in refinement/test set	42190/2123	23858/1211	39028/1994	23603/1207	39990/2050
R _{work} /R _{free} (%) ^{a,c}	18.7/21.7 (24.0/30.8)	18.8/22.1 (24.6/28.2)	13.4/16.1 (22.6/25.5)	17.1/21.0 (21.7/25.6)	14.6/16.2 (40.0/46.1)
twining fraction	0	0	0.25	0	0.42
twin law	N/A	N/A	h, -h-k, -l	N/A	h, -h-k, -l
no. of atoms ^d					
protein	4571	2288	2231	2235	2212
solvent	265	93	160	178	122
Mn ²⁺	4	2	0	2	2
glycerol	6	0	0	0	0
root-mean-square deviation					
bonds (Å)	0.006	0.009	0.008	0.008	0.008
angles (deg)	0.9	1.1	1.1	1.1	1.2
average B factor (Å ²)					
main chain	27	35	16	24	21
side chain	29	37	20	27	23
solvent	32	38	24	30	24
metal ions	26	29	N/A	23	19
Ramachandran plot (%)					
allowed	91.1	89.8	91.4	90.7	90.2
additionally allowed	8.9	10.2	8.2	9.3	9.3
generously allowed	0.0	0.0	0.4	0.0	0.4
disallowed	0.0	0.0	0.0	0.0	0.0

^aValues in parentheses refer to the highest resolution shell. ^bR_{sym} = $\sum_h \sum_i |I(h)_i - \langle I(h) \rangle| / \sum_h \sum_i I(h)_i$, where $I(h)$ is the intensity of reflection h , \sum_h is the sum over all reflections and \sum_i is the sum over i measurements of reflection h . ^cR_{work} = $\sum ||F_o| - |F_c|| / \sum |F_o|$ for reflections contained in the working set. R_{free} = $\sum ||F_o| - |F_c|| / \sum |F_o|$ for reflections contained in the test set held aside during refinement (5% of total). $|F_o|$ and $|F_c|$ are the observed and calculated structure factor amplitudes, respectively. ^dPer asymmetric unit.

5'-CCG ACA GAG GTG GGG CAA CAT CCA AAT GAG-3' (antisense). Mutations were verified by DNA sequencing.

TcFIGase was overexpressed in *E. coli* BL21(DE3) cells in Lysogeny-Broth (LB) media or M9 minimal media (1× M9 salts, 10% casamino acids, 20 mM D-(+)-glucose, 2 mM MgSO₄, 100 μM CaCl₂) supplemented with 100 mg/L ampicillin. Expression was induced by 1 mM isopropyl β-D-1-thiogalactopyranoside (IPTG) (Carbosynth) for 16 h at 22 °C when the OD₆₀₀ reached 0.6–0.7. For minimal media growth, 100 μM MnCl₂ was added into the culture 30 min before induction. Cells were harvested by centrifugation at 5000g for 10 min. The cell pellet was suspended in 50 mL of buffer A (50 mM K₂HPO₄ (pH 8.0), 300 mM NaCl, 10% (v/v) glycerol, 1 mM TCEP). Cells were lysed by sonication on ice using a Sonifer 450 (Branson), and the cell lysate was further incubated with 5 μg/mL DNase I (Sigma) and 6 μg/mL RNase A (Roche Applied Science) at 4 °C for 30 min. Cellular debris was removed by centrifugation at 26895g for 1 h. The clear supernatant was applied to a Talon column (Clontech Laboratories, Mountain View, CA) pre-equilibrated with buffer

A. TcFIGase was purified with a 200 mL gradient from 10 mM imidazole to 300 mM imidazole. Pooled fractions were dialyzed into buffer B (20 mM K₂HPO₄ (pH 8.0), 2 mM β-mercaptoethanol (BME) and 100 μM MnCl₂) and subsequently loaded onto a 10 mL Q-HP anion exchange column (GE Healthcare). Protein was eluted with a 500 mL gradient from 0 mM NaCl to 800 mM NaCl. Estimated purity of protein samples was >95% based on SDS-PAGE. Fractions containing TcFIGase were combined and concentrated using Amicon ultra filter units (Millipore) with a 10 kDa molecular weight cutoff followed by buffer exchange into buffer C (50 mM bicine (pH 8.5), 100 μM MnCl₂, 1 mM TCEP) using PD-10 columns (GE Healthcare). Mutants were expressed in minimal media and purified as described for the wild-type enzyme. Oxidized TcFIGase (TcFIGase_{ox} bearing a disulfide linkage between C35 and C242) was serendipitously obtained by purifying the enzyme in the absence of reducing agent.

Attempts to use metal chelators such as EDTA and dipicolinic acid (DPA) to remove metal ions from wild-type enzyme were

not successful. Apo-TcFIGase was prepared by gradually lowering the pH to 4.2 through stepwise dialysis: 20 mM *N*-(2-hydroxyethyl)piperazine-*N'*-(3-propanesulfonic acid) was used in the pH range 6.5–7.5; 20 mM 2-(*N*-morpholino)ethanesulfonic acid was used in the pH range 5.5–6.5; and 20 mM sodium acetate was used in the pH range 4.2–5.5. Routinely, 5 mM BME was included in all dialysis buffers to prevent oxidation. Metal-depleted TcFIGase was then buffer-exchanged into Chelex resin pretreated buffer D (10 mM Tris-HCl (pH 8.0), 1 mM TCEP) by dialysis. Apo-TcFIGase was concentrated to 30 mg/mL, flash frozen by liquid nitrogen, and stored at -80°C .

Enzyme concentrations were determined by the Bradford assay.²³ Metal content was quantified by inductively coupled plasma-atomic emission spectrometry (ICP-AES) at the Center for Applied Isotope Studies, University of Georgia (Athens, GA). Samples were extensively dialyzed against 10 mM bicine (pH 8.5) to remove free trace metal ions prior to analysis by ICP-AES.

Crystallography. Crystals of TcFIGase were prepared by the hanging drop vapor diffusion method at 21°C . For TcFIGase_{ox} and N114H TcFIGase, a 4 μL drop of protein solution [10 mg/mL protein, 50 mM bicine (pH 8.5), 100 μM MnCl_2] was mixed with a 4 μL drop of precipitant solution [25% PEG 3350, 0.1 M sodium acetate (pH 4.6)] on a siliconized cover slide and equilibrated against a 500 μL reservoir of precipitant solution. For wild-type TcFIGase, a 4 μL drop of protein solution [10 mg/mL protein, 50 mM bicine (pH 8.5), 100 μM MnCl_2 , 1 mM TCEP] was mixed with a 4 μL drop of precipitant solution [31% PEG 300, 0.1 M sodium acetate (pH 4.9)] on a siliconized cover slide and equilibrated against a 500 μL reservoir of precipitant solution. Crystals first appeared after 2 days and grew to maximum size in 1 week. To obtain crystalline metal-bound enzyme, crystals of the apoenzyme were successively soaked with 5–20 mM MnCl_2 in the corresponding precipitant solution with gradually increasing pH (in the pH range 6.0–8.5, 0.1 M sodium acetate was replaced by 0.1 M sodium malonate). Crystals were flash-cooled after transfer to a cryoprotectant solution consisting of the soaking solution augmented with 15–20% glycerol. Diffraction data were collected on our home X-ray source (Rigaku IV++ image plate area detector mounted on a Rigaku RU200HB rotating anode X-ray generator) and on beamline X29 at the National Synchrotron Light Source (NSLS, Brookhaven National Laboratory, New York). Diffraction data were integrated and scaled with HKL2000.²⁴ In comparison with the structure of the arginase superfamily protein deposited in the PDB by the Structural Genomics of Pathogenic Protozoa Consortium (PDB entry 2A0M), crystals of N114H Mn^{2+} -TcFIGase and Mn^{2+} -TcFIGase_{ox} (pH 6.0) similarly belonged to space group *H*3 and exhibited nearly identical unit cell parameters; crystals of Mn^{2+} -TcFIGase were similarly isomorphous except for a *c*-axis doubled in length, and crystals of apo-TcFIGase_{ox} and Mn^{2+} -TcFIGase_{ox} (pH 8.5) were similarly isomorphous except for partial twinning. The doubled unit cell volume indicated that the asymmetric unit contained two monomers. A significant off-origin peak (84% of the origin peak) in the Patterson function (calculated with phenix.xtriage²⁵) suggested that the two monomers were related by pseudotranslational symmetry. However, satisfactory solutions were generated for the rotation and translation functions in molecular replacement calculations, and structure refinement proceeded smoothly. Data collection and reduction statistics are listed in Table 1. Structures were determined by molecular replacement using the program PHASER,²⁶ as implemented in the CCP4

suite,²⁷ with the coordinates of wild-type apo-TcFIGase less ligand and solvent molecule as a search model. The degree of crystal twinning was assessed using the program phenix.xtriage.²⁵ Iterative cycles of refinement and model building were performed using PHENIX²⁵ and COOT.²⁸ Solvent molecules were added in the final stages of refinement for each structure. Disordered segments not included in the final models include the N-terminus (M1-T5 in Mn^{2+} -TcFIGase and apo-TcFIGase_{ox}; M1-R4 in N114H Mn^{2+} -TcFIGase and Mn^{2+} -TcFIGase_{ox} (pH 6.0 and 8.5)), the C-terminus (K303–N308 in all structures), L147–G155 in apo-TcFIGase_{ox}, P146–S154 in Mn^{2+} -TcFIGase_{ox} at pH 6.0, and P145–S154 in Mn^{2+} -TcFIGase_{ox} at pH 8.5. The side chain of active site residue C242 is disordered such that its *S*_γ atom occupies two positions in the final models of Mn^{2+} -TcFIGase and N114H Mn^{2+} -TcFIGase. Bijvoet difference Fourier maps were calculated with PHENIX.²⁵ The quality of each final model was verified with PROCHECK and secondary structure was defined with DSSP.^{29,30} Refinement statistics are reported in Table 1.

Activity Assays. Ureohydrolase activity was monitored spectrophotometrically on the basis of the formation of urea using the colorimetric assay developed by Archibald.³¹ Briefly, 20 mM guanidino substrate was added to a solution of 50 mM 4-(2-hydroxyethyl)piperazine-1-propanesulfonic acid (pH 8.5), and the reaction was initiated by adding 100 μM TcFIGase in a total volume of 200 μL . The reaction was terminated after 1 h using 30 μL of a 3:1 (v/v) concentrated acid/dye solution [H_2SO_4 : H_3PO_4 : H_2O (1:3:1 v/v/v)/245 mM α -isonitrosopropiophenone in ethanol]. Samples were heated to 90°C for 1 h in a thermocycler to ensure complete reaction of urea with the dye. Absorbance was measured at $\lambda = 550\text{ nm}$ using an Agilent HP 8452A Diode Array spectrophotometer.

L-Formiminoglutamase activity was monitored colorimetrically at 22°C based on the protocol developed by Lund and Magasanik.²¹ Typically, 0.2 mL assay buffer [20 mM 1,3-bis(tris(hydroxymethyl)methylamino)propane, 20 mM *N*-cyclohexyl-3-aminopropanesulfonic acid (pH 9.5)] containing enzyme (5–100 μM) was initiated by the addition of substrate L-formiminoglutamic acid (2–20 mM). The reaction was stopped by addition of 0.8 mL saturated sodium borate solution, followed by 0.2 mL of the chromophore reagent (4 g of sodium nitroprusside, 4 g of potassium ferricyanide, and 4 g of NaOH in 140 mL H_2O). Absorbance was measured at $\lambda = 485\text{ nm}$ after 30 min. All measurements were made in triplicate. Kinetic constants were calculated by fitting initial velocity data to either the Michaelis–Menten equation or the Hill equation using Origin-Pro 8.0 and are reported as mean \pm standard deviation.

Metallo-substituted enzyme was prepared by incubating the apoenzyme with metal ions (2 mM MgCl_2 , CaCl_2 , MnCl_2 , CoCl_2 , NiCl_2 , CuCl_2 , ZnCl_2 , FeCl_2 , or FeCl_3) in 50 mM bicine (pH 8.5) and 2 mM TCEP on ice for at least 1 h prior to dilution into assay buffer. All work with Fe^{2+} was performed anaerobically under a nitrogen atmosphere in an AtmosBag (Sigma). Dissolved oxygen was removed from dd H_2O by sparging with N_2 .

RESULTS

Tertiary and Quaternary Structure. As previously found for the protein of undetermined function annotated as “arginase superfamily protein” from *Trypanosoma cruzi* by the Structural Genomics of Pathogenic Protozoa Consortium²⁰ (PDB entry 2A0M), TcFIGase adopts the classic α/β arginase-deacetylase fold¹⁵ comprised of an eight-stranded parallel β -sheet (strand order 21387456) flanked by numerous α -helices (Figure 2a).

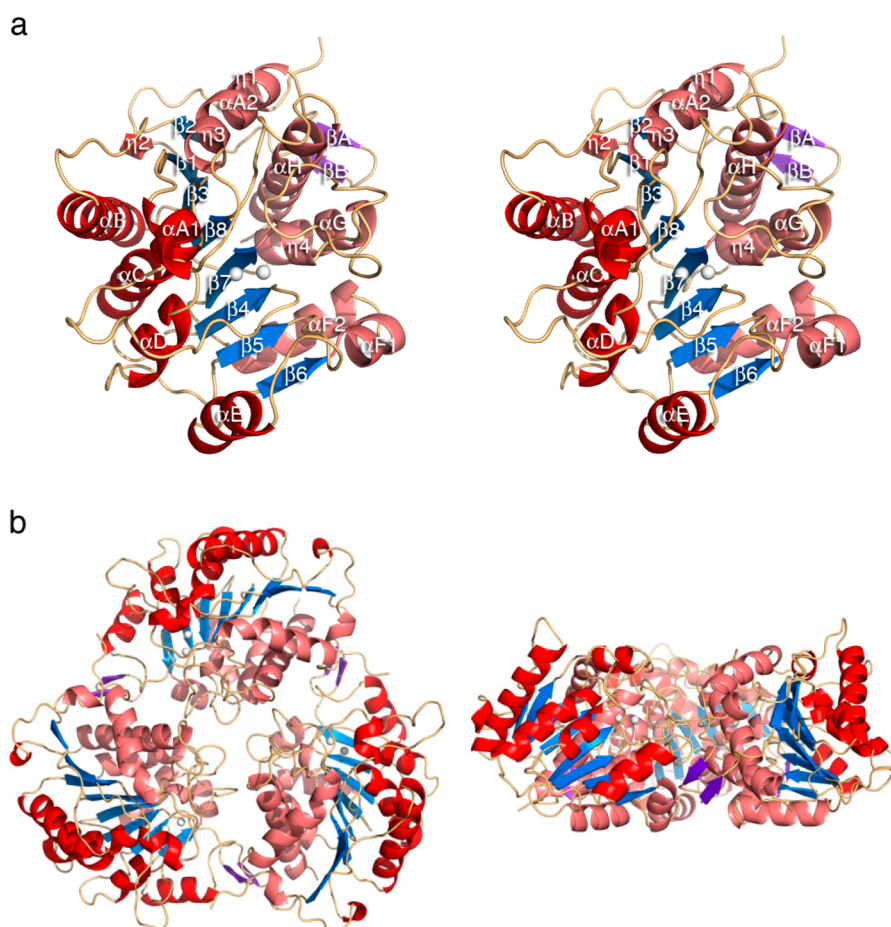


Figure 2. (a) Stereoview of the Mn^{2+} -TcFIGase monomer. Secondary structure elements are defined by DSSP;³⁰ α -helices are red and β -strands are blue (β strands 1–8) or purple (β -strands βA and βB). The Mn^{2+} ions are shown as white spheres. (b) Top view (left) and side view (right) of the Mn^{2+} -TcFIGase trimer.

Helices $\eta 2$, A1, B, C, D, and E reside on one face and helices $\eta 1$, A2, $\eta 3$, F1, F2, $\eta 4$, G, and H reside on the other face of the central β -sheet. Two additional β -strands (βA and βB) are inserted between helix A2 and strand $\beta 2$ to form a protruding β -hairpin, which contributes to the interface between monomers. The G111-G112 *cis*-peptide bond, which is contained in the widely conserved GGDH motif in the ureohydrolase family, is also conserved in TcFIGase and lies at the edge of strand $\beta 3$. This *cis*-peptide bond is believed to be important for positioning active site residues N114 and E277, known to be important for catalytic function as implicated in other ureohydrolases.¹⁹ Similar to eukaryotic arginases,^{15,32–35} TcFIGase adopts a trimeric quaternary structure (Figure 2b). The buried solvent accessible surface area is 1884 Å² between each monomer of the assembled homotrimer as determined by PISA.³⁶ In contrast with the eukaryotic arginases, in which the S-shaped C-terminal polypeptide dominates intermonomer contacts in the trimer, the N-terminus of TcFIGase makes significant intermonomer interactions, which is more similar to trimer assembly in proclavaminic acid amidinohydrolase,¹⁶ agmatinase,¹⁷ guanidinobutyrase, and guanidinopropionase.¹⁸

Active Site Structure. The crystallization of TcFIGase exclusively yields the metal-free apoenzyme due to the fact that it crystallizes only at very low pH (pH < 5). This accounts for the complete lack of active site metal ions in the 1.6 Å resolution crystal structure determined by the Structural Genomics of Pathogenic Protozoa Consortium²⁰ and the resultant misanno-

tation of the protein (PDB entry 2A0M). To obtain the crystal structure of the metal-bound enzyme, crystals of wild-type TcFIGase were soaked with 5 mM MnCl_2 at pH 8.0. The binding of two Mn^{2+} ions in the active site was confirmed by two strong peaks in the Bijvoet difference Fourier map shown in Figure 3a. Each Mn^{2+} ion is coordinated with octahedral or distorted-octahedral geometry: the $\text{Mn}^{2+}_{\text{A}}$ ion is coordinated by N114 O δ , D138 O $\delta 2$, D142 O $\delta 2$, D228 O $\delta 2$, and two solvent molecules, one of which bridges $\text{Mn}^{2+}_{\text{A}}$ and $\text{Mn}^{2+}_{\text{B}}$ and donates a hydrogen bond to D142 O $\delta 1$; the $\text{Mn}^{2+}_{\text{B}}$ ion is coordinated by H140 N δ , D228 O $\delta 2$, D138 O $\delta 1$, D230 O $\delta 1$ and O $\delta 2$ in symmetric bidentate fashion, and the metal-bridging solvent molecule. Metal binding does not cause any global conformational changes, and the root-mean-square (rms) deviation between apo-TcFIGase and Mn^{2+} -TcFIGase is 0.18 Å for 278 C α atoms as calculated with MacPymol.³⁷ However, metal binding triggers some local structural changes in the active site, in that metal ligands undergo varying degrees of conformational changes to enable inner-sphere coordination of $\text{Mn}^{2+}_{\text{A}}$ and $\text{Mn}^{2+}_{\text{B}}$ (Figure 3b). In contrast, relatively minimal conformational changes accompany metal binding to the metal-free ureohydrolases agmatinase from *D. radiodurans* and human arginase I.^{17,38} It is possible, however, that the alternative conformations observed for metal ligands in apo-TcFIGase result from the low pH of the apoenzyme crystal structure determination.

Interestingly, the conformation of N114 in Mn^{2+} -TcFIGase is comparable to that of N101 in the 2.5 Å resolution crystal

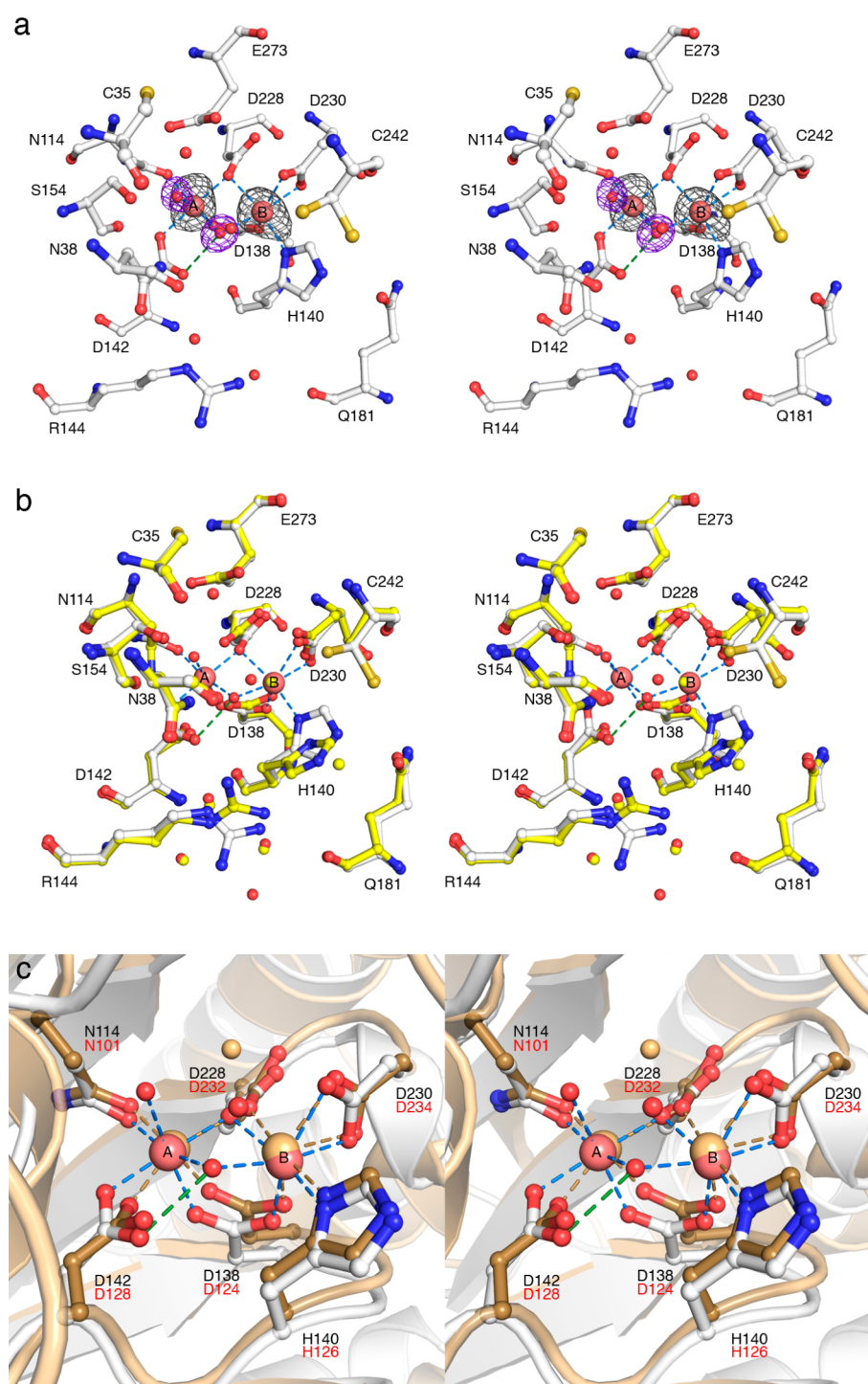


Figure 3. (a) Bijvoet difference Fourier map (gray, contoured at 5σ) of Mn^{2+} ions and simulated annealing omit map (blue, contoured at 4σ) of Mn^{2+} -bound solvent molecules in the active site of Mn^{2+} -TcFIGase (pH 8.0). Atoms are color-coded as follows: C = white, N = blue, O = red, Mn^{2+} = pink spheres, solvent = red spheres. Metal coordination and hydrogen bond interactions are represented by blue and green dashed lines, respectively. Note that the side chain thiol group of C242 is disordered between two positions. (b) Superposition of Mn^{2+} -TcFIGase (color coded as in (a)) and apo-TcFIGase (PDB entry 2A0M, color coded as in (a) except that C = yellow). (c) Superposition of Mn^{2+} -TcFIGase (color coded as in (a)) and H101N rat arginase I (PDB entry 1P8P, tan). TcFIGase and rat arginase I residue labels are black and red, respectively.

structure of H101N rat arginase I (PDB entry 1P8P, which updated a previous structure determination (PDB entry 3RLA) in which the metal ligand was not characterized by well-defined electron density).^{39,40} The superposition of Mn^{2+} -TcFIGase and H101N rat arginase I reveals almost identical metal coordination geometries, with the exception that in H101N rat

arginase I the Mn^{2+}_A site is only half-occupied and nonprotein ligands (solvent molecules) are not observed, probably due to the lower resolution of the structure determination (Figure 3c). The Mn^{2+}_A - Mn^{2+}_B separation of 3.2 Å in Mn^{2+} -TcFIGase is comparable to that observed in H101N rat arginase I (3.1 Å) as well as the Mn^{2+}_A - Mn^{2+}_B separations generally observed in wild-

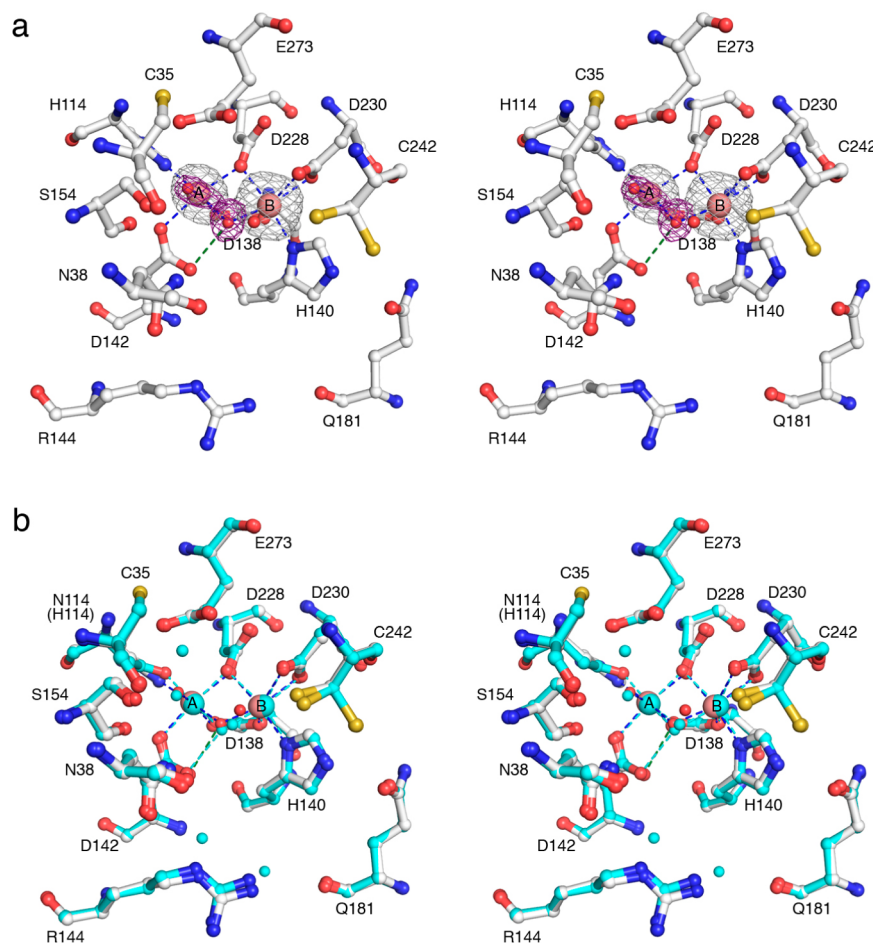


Figure 4. (a) Simulated annealing omit maps of Mn²⁺ ions (gray, contoured at 3 σ) and metal-bound solvent molecules (purple, contoured at 5 σ) in the active site of N114H Mn²⁺-TcFIGase (pH 7.5). Atoms are color-coded as follows: C = white, N = blue, O = red, Mn²⁺ = pink spheres, solvent = red spheres. Metal coordination and hydrogen bond interactions are represented by blue and green dashed lines, respectively. Note that the side chain thiol group of C242 is disordered between two positions. (b) Superposition of N114H Mn²⁺-TcFIGase (color coded as in (a)) and wild-type Mn²⁺-TcFIGase (color coded as in (a) except that C, Mn²⁺ = cyan).

type ureohydrolases.^{15–18,32–35} In Mn²⁺-TcFIGase, the Mn²⁺_A ion is coordinated by N114 O δ with a separation of 2.2 Å; in H101N rat arginase I, the corresponding N101 O δ –Mn²⁺_A separation is 2.1 Å. Additionally, “second shell” interactions are similar in both enzymes. In TcFIGase, the N114 N δ -H groups donate hydrogen bonds to the side chain hydroxyl group of S117 and a water molecule; in turn, this water molecule hydrogen bonds with the side chains of S226 and N136. In H101N rat arginase I, the N101 N δ -H group donates a hydrogen bond to a water molecule, which in turn hydrogen bonds with S230.

Structure of N114H TcFIGase. To restore the characteristic metal binding motif found in most binuclear metalloureohydrolases (i.e., to engineer the metal cluster of TcFIGase so as to resemble that of arginase),^{15,33} N114H TcFIGase was prepared. The 1.80 Å resolution X-ray crystal structure of this mutant reveals a nearly fully occupied binuclear manganese cluster (Mn²⁺_A occupancy = 75%, Mn²⁺_B occupancy = 100%), as confirmed in the simulated annealing omit map of Figure 4a. The side chain N δ atom of H114 coordinates to Mn²⁺_A with a separation of 2.2 Å, and the N ϵ -H group is a bifurcated hydrogen bond donor to the side chain hydroxyl groups of S117 and S226. In rat arginase I and human arginase I, a single serine residue, S230, accepts a hydrogen bond from the N ϵ -H group of the corresponding Mn²⁺_A ligand, H101.^{15,41} The manganese

coordination polyhedra are otherwise unchanged compared with wild-type TcFIGase (Figure 4b) and resemble those observed in other unliganded ureohydrolases, including *B. caldovelox* arginase,⁴² *L. mexicana* arginase,³⁵ *S. clavuligerus* proclavaminic acid amidinohydrolase,¹⁶ *P. aeruginosa* guanidinopropionase, and *P. aeruginosa* guanidinobutyrase.¹⁸

Structure of Oxidized TcFIGase (TcFIGase_{ox}). When apo-TcFIGase is prepared and crystallized in the absence of reducing agents, the 1.53 Å-resolution structure reveals the formation of a disulfide linkage between C35 and C242 in the active site. The metal-bound form of this oxidized protein, Mn²⁺-TcFIGase_{ox}, is prepared by soaking apoenzyme crystals in a buffer solution containing 20 mM MnCl₂. The 1.8 Å-resolution crystal structure of metal-bound TcFIGase_{ox} determined at pH 6.0 reveals one strong peak and one weak peak in the Bijvoet difference Fourier map—the Mn²⁺_B site is fully occupied and the Mn²⁺_A site is 40% occupied (Figure 5a). The overall structure of metal-bound TcFIGase_{ox} is generally similar to that of Mn²⁺-TcFIGase, with an rms deviation of 0.13 Å for 241 C α atoms. However, two major conformational changes are triggered by disulfide bond formation (Figure 5b): first, helix A1 (E33–R37, which contains C35 in the disulfide linkage) and its flanking loops shift ~4 Å toward the active site; second, the surface loop P146–S154 becomes disordered. As a result of these conformational changes,

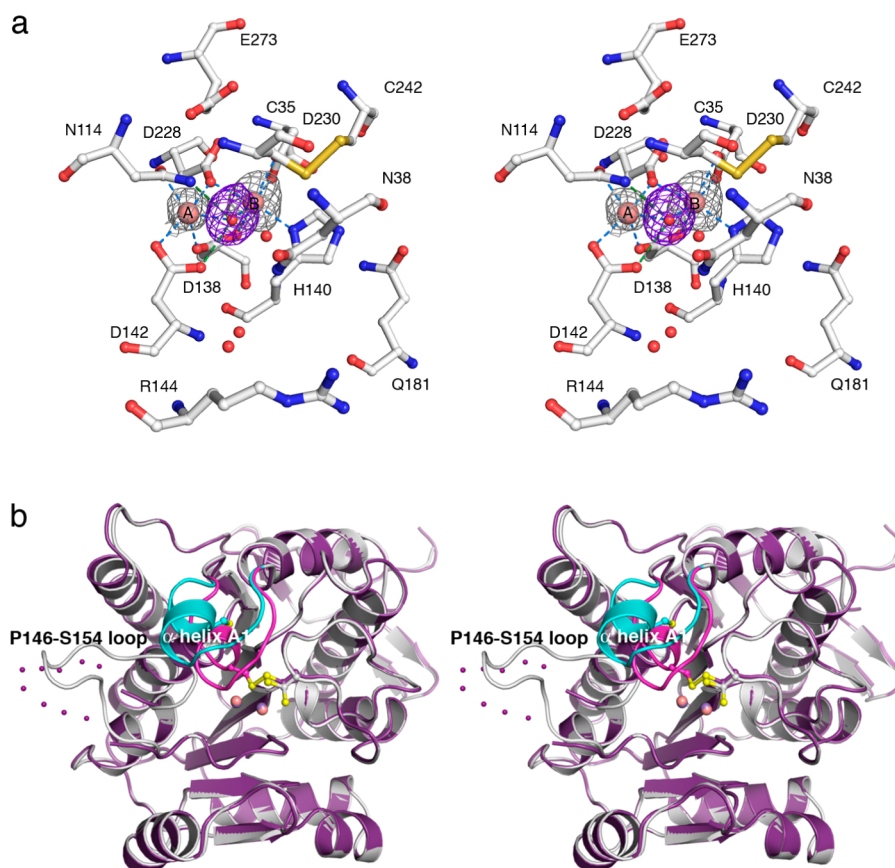


Figure 5. (a) Bijvoet difference Fourier map (gray, contoured at 3σ) of Mn^{2+} ions and simulated annealing omit map (purple, contoured at 3σ) of Mn^{2+} -bound solvent molecules in the active site of wild-type Mn^{2+} -TcFIGase_{ox} (pH 6.0). Atoms are color-coded as follows: C = white, N = blue, O = red, Mn^{2+} = pink spheres, solvent = red spheres. Metal coordination and hydrogen bond interactions are represented by blue and green dashed lines, respectively. (b) Superposition of the Mn^{2+} -TcFIGase_{ox} monomer (pH 6.0, purple) and the Mn^{2+} -TcFIGase monomer (white); dotted lines indicate disordered polypeptide segments. Major conformational changes occur for helix A1 (dark pink (oxidized state), cyan (reduced state)) and the P146–S154 loop in response to disulfide bond formation.

the original entrance to the active site is partially blocked by helix A1 (especially by N38 and the C35–C242 disulfide linkage). However, two possible alternative entrances are formed as calculated with the program MOLE:⁴³ one is adjacent to the original entrance and results from the shift of R144, and the second results from the disorder of the P146–S154 loop (Figure 6a). Comparison of the atomic displacement parameters of Mn^{2+} -TcFIGase (pH 8.0) and Mn^{2+} -TcFIGase_{ox} (pH 8.5) reveals that loop P146–S154 and helix A1 exhibit significant flexibility in both structures (Figure 6b). Therefore, disulfide bond formation appears to be a fortuitous consequence of this flexibility. The geometry of the C35–C242 disulfide linkage is +LHSpiral as defined by Schmidt and colleagues,⁴⁴ which is not characteristic of any particular function.

Notably, the binuclear metal cluster is influenced by disulfide bond formation in TcFIG_{ox} (Figure 7a). Although the $\text{Mn}^{2+}_{\text{A}}$ – $\text{Mn}^{2+}_{\text{B}}$ separation remains at 3.1 Å and the N114 O δ atom remains coordinated to $\text{Mn}^{2+}_{\text{A}}$, the occupancy of $\text{Mn}^{2+}_{\text{A}}$ is reduced to 40%. Additionally, the second water molecule coordinated to $\text{Mn}^{2+}_{\text{A}}$ as the sixth ligand in the structure of Mn^{2+} -TcFIGase is sterically displaced by the N δ -H group of N114, which donates a hydrogen bond to the metal-bridging solvent molecule; while the N114 N δ atom is 3.0 Å away from E273, it is poorly oriented for hydrogen bond formation. The N δ atom of N114 is also 2.5 Å away from $\text{Mn}^{2+}_{\text{A}}$, which is too long

for an inner-sphere coordination interaction that would also require the unlikely ionization of the carboxamide side chain.

To increase the occupancy of $\text{Mn}^{2+}_{\text{A}}$, crystals of apo-TcFIGase_{ox} were soaked in a buffer solution containing 20 mM MnCl_2 at pH 8.5. However, the resulting crystal structure reveals that although $\text{Mn}^{2+}_{\text{B}}$ remains fully bound, $\text{Mn}^{2+}_{\text{A}}$ binds with only 30% occupancy (Figure 7b). Intriguingly, lower $\text{Mn}^{2+}_{\text{A}}$ occupancy is accompanied by the conformational change of former $\text{Mn}^{2+}_{\text{A}}$ ligand D142, which swings away from the metal site to accept hydrogen bonds from N38 and R144. Consequently, a solvent molecule coordinates to $\text{Mn}^{2+}_{\text{A}}$ at the site formerly occupied by D142. The flexibility of D142 could be mediated in part by its proximity to the highly flexible P146–S154 loop (Figure 6b). Other changes observed in the structure include a shorter $\text{Mn}^{2+}_{\text{A}}$ – $\text{Mn}^{2+}_{\text{B}}$ separation of 2.9 Å and asymmetric metal coordination by the bridging solvent molecule with $\text{Mn}^{2+}_{\text{A}}$ –O and $\text{Mn}^{2+}_{\text{B}}$ –O separations of 2.1 Å and 2.4 Å, respectively. The N114 O δ – $\text{Mn}^{2+}_{\text{A}}$ interaction is weakened with a separation of 2.6 Å, which is too long to be considered inner-sphere metal coordination.

Metal Content Analysis. The metal ion content of TcFIGase was measured using inductively coupled plasma-atomic emission spectrometry (ICP-AES) (Table 2). Both wild-type TcFIGase and N114H TcFIGase, as expressed and purified from LB media, exhibit heterogeneity in terms of their metal ion content: each contains nearly one equivalent Mn^{2+} per

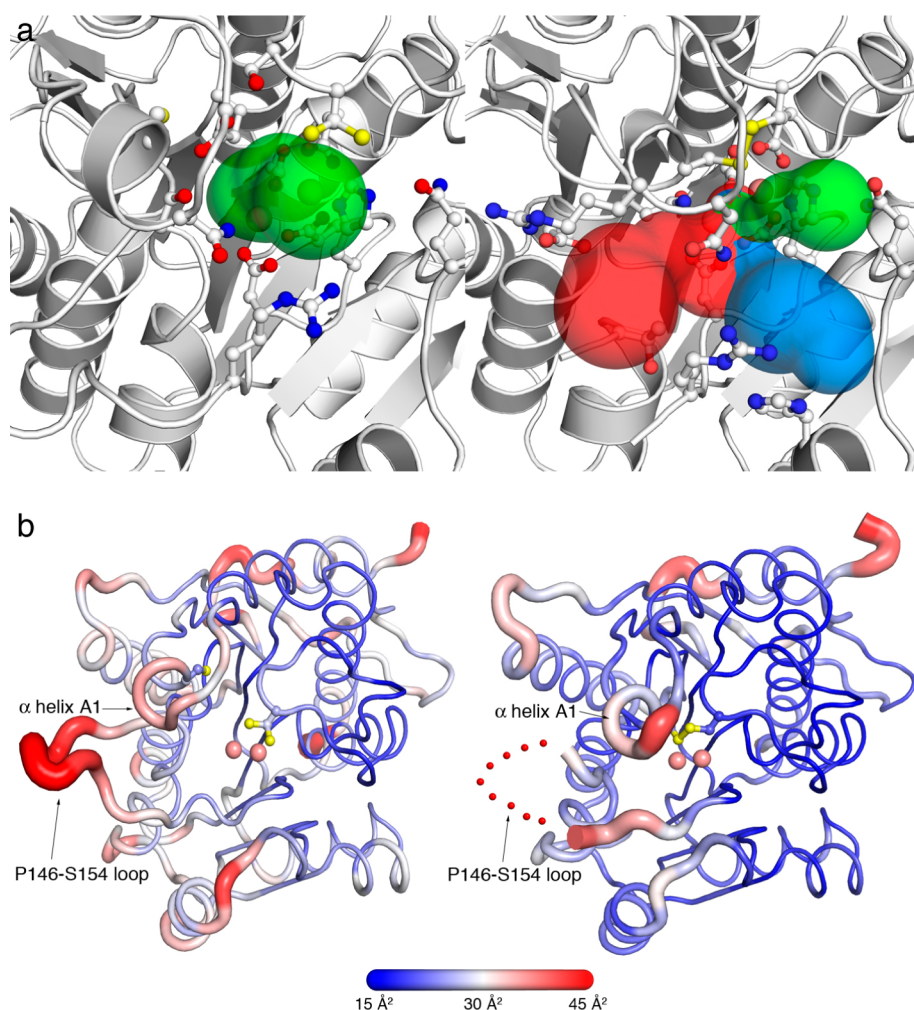


Figure 6. (a) Structural changes in active site access triggered by disulfide bond formation in Mn^{2+} -TcFIGase. The original active site entrance is indicated by a green surface (left image). Following disulfide bond formation in Mn^{2+} -TcFIGase_{ox}, this entrance becomes constricted and two new entrances (blue and red surfaces) become accessible (right image). Selected residues lining the entrance surface are shown as stick figures and Mn^{2+} ions are shown as pink spheres. Active site entrance surfaces were calculated using MOLE.⁴³ (b) Cartoon representation of Mn^{2+} -TcFIGase (pH 8.0, left) and Mn^{2+} -TcFIGase_{ox} (pH 8.5, right), showing the atomic displacement parameters coded by thickness of the main chain and a color gradient from blue (low disorder) to red (high disorder). The red-dotted line indicates the disordered P146–S154 loop.

monomer, but wild-type TcFIGase is contaminated with Fe^{2+} and N114H TcFIGase is contaminated with Co^{2+} . To minimize the contamination by adventitious divalent metal ions, expression of wild-type TcFIGase from minimal media supplemented with MnCl_2 results in the incorporation of only one equivalent of Mn^{2+} into each monomer. The metal ion content of TcFIGase_{ox} is comparable to that found in the reduced form, TcFIGase. Notably, ICP-AES analysis suggests that only one site in the binuclear metal cluster binds Mn^{2+} tightly in solution. Based on the crystallographic studies outlined in the previous section, it is likely that this corresponds to the Mn^{2+}_B ion; it is possible that the Mn^{2+}_A ion is bound more weakly than the Mn^{2+}_B ion under physiological conditions.

Measurement of Enzyme Kinetics. To evaluate the possibility that TcFIGase might exhibit ureohydrolase activity, given its structural similarity to arginase and other related ureohydrolases, different guanidinium derivatives were tested as potential substrates using the colorimetric ureohydrolase assay developed by Archibald.³¹ However, no urea formation was detected in assays that would have detected 0.4 micromoles of urea formed per minute with the following substrates: L-arginine,

agmatine, L-acetylarginine, α -guanidinoglutaric acid, L-homo-arginine, L-2-amino-3-guanidinopropionic acid, 3-guanidinopropionic acid, and 4-guanidinobutyric acid.

Instead, TcFIGase exclusively exhibits formiminoglutamase activity as measured using the colorimetric L-formiminoglutamate assay developed by Lund and Magasanik (Table 3).²¹ Wild-type TcFIGase expressed and purified from LB media displays the following steady-state kinetic parameters: $k_\text{cat} = 200 \pm 20 \text{ s}^{-1}$, $K_\text{M} = 40 \pm 10 \text{ mM}$, and $k_\text{cat}/K_\text{M} = 5200 \pm 200 \text{ M}^{-1} \text{ s}^{-1}$. The catalytic efficiency (k_cat/K_M) is approximately 2-fold higher than that of metal-free wild-type TcFIGase reconstituted exclusively with Mn^{2+} , which exhibits $k_\text{cat} = 110 \pm 20 \text{ s}^{-1}$, $K_\text{M} = 50 \pm 10 \text{ mM}$, and $k_\text{cat}/K_\text{M} = 2300 \pm 300 \text{ M}^{-1} \text{ s}^{-1}$. While the K_M value measured for TcFIGase is somewhat high, it is comparable to that measured for the formiminoglutamases from *Aerobacter aerogenes* ($K_\text{M} = 40 \text{ mM}$ at pH 8.5) and *Bacillus subtilis* ($K_\text{M} = 39 \text{ mM}$ at pH 7.4).^{21,22} These values are, however, higher than the K_M value of 4.3 mM measured for formiminoglutamase from *Pseudomonas aeruginosa*.⁴⁵ Nevertheless, these results confirm that the protein of undetermined function annotated as “arginase superfamily protein” from *Trypanosoma cruzi* by the Structural

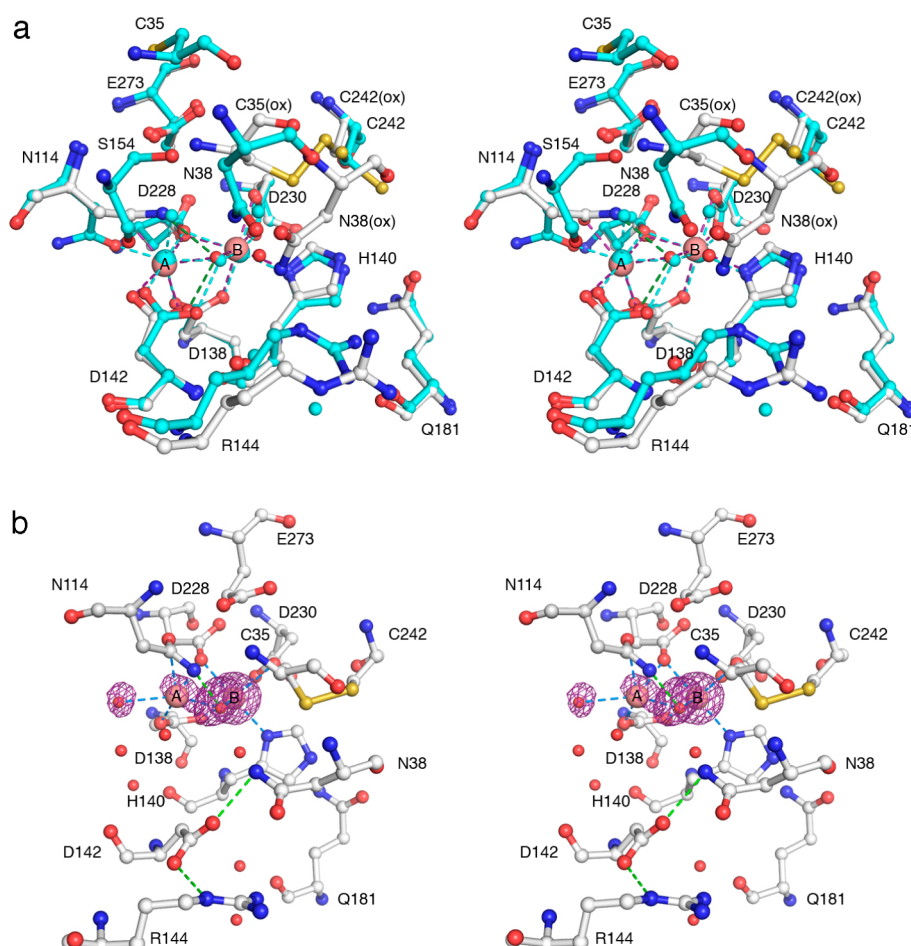


Figure 7. (a) Close-up view of active site from the superposition of Mn^{2+} -TcFIGase_{ox} (C = white) with Mn^{2+} -TcFIGase (C = cyan). Metal coordination and hydrogen bond interactions in Mn^{2+} -TcFIGase_{ox} are represented by red and green dashed lines, respectively. (b) Simulated annealing omit maps (purple, contoured at 3σ) of Mn^{2+} ions and Mn^{2+} -bound solvent molecules observed in Mn^{2+} -TcFIGase_{ox} soaked in a buffer solution containing 20 mM MnCl_2 at pH 8.5. Atoms are color-coded as follows: C = white, N = blue, O = red, Mn^{2+} = pink spheres, solvent = red spheres. Metal coordination and hydrogen bond interactions are represented by blue and green dashed lines, respectively. Note the reduced Mn^{2+} occupancy and conformational change of former Mn^{2+} ligand D142.

Table 2. Metal Content Analysis

	metal/protein molar ratio							
	Mn	Fe	Co	Ni	Cu	Zn	Mg	Ca
wild-type TcFIGase	0.84	0.22	0.04	0.003	0.008	0.04	0.005	0.01
N114H TcFIGase	0.85	0.03	0.24	0.004	0.004	0.03	0.08	0.03
wild-type TcFIGase after treatment with metal ion chelators ^a	0.80	0.31	0.05	0.002	0.005	0.01	0.003	0.04
wild-type TcFIGase, pH 4.2 ^b	0.11	0.20	0.04	0.0002	0.002	0.008	n.d. ^c	0.01
wild-type TcFIGase _{ox}	0.84	0.14	0.08	0.0014	0.004	0.02	n.d.	0.004
wild-type TcFIGase, minimal media + MnCl_2 ^d	1.05	0.02	0.03	0.0004	n.d.	0.03	0.10	0.001

^aTreatment with 55 mM DPA and 80 mM EDTA for 24 h; chelators were then dialyzed prior to analysis. ^bThe pH was gradually lowered to 4.2 by dialysis and then raised to 8.0 for ICP-AES. ^cn.d., not detected. ^dProtein expressed and purified from minimal media supplemented with 100 μM MnCl_2 upon induction.

Genomics of Pathogenic Protozoa Consortium²⁰ (PDB entry 2A0M) is in fact a formiminoglutamase.

The oxidized form of the wild-type enzyme, TcFIGase_{ox}, exhibits 67% catalytic efficiency compared to wild-type TcFIGase. The slightly lower activity of TcFIGase_{ox} could be a consequence of the narrowed active site entrance. Regardless, formation of the C35–C242 disulfide linkage does not appear to have a significant influence on catalysis. Neither of these cysteine residues are conserved among formiminoglutamases from

different species and are instead substituted by small aliphatic amino acids residues (mainly valine and alanine) (Figure 8). Hence, the C35–C242 disulfide linkage is probably an artifact rather than a functional allosteric linkage for the regulation of enzyme activity.

The restoration of an authentic, “arginase-like” Mn^{2+} coordination polyhedron does not significantly affect catalysis: N114H TcFIGase exhibits 65% catalytic efficiency compared to wild-type TcFIGase (Table 3). Thus, asparagine and histidine

Table 3. Steady-State Kinetics at pH 9.5

enzyme	k_{cat} (s ⁻¹)	K_M (mM)	k_{cat}/K_M (M ⁻¹ s ⁻¹)
wild-type TcFIGase ^a	200 ± 20	40 ± 10	5200 ± 200
wild-type TcFIGase _{ox} ^a	140 ± 20	40 ± 20	3500 ± 200
wild-type TcFIGase ^b	140 ± 40	100 ± 30	1400 ± 200
N114H TcFIGase ^a	80 ± 10	20 ± 10	3400 ± 200
R144E TcFIGase ^{b,d}	0.05 ± 0.02	9 ± 4	5.2 ± 0.6
R144A TcFIGase ^b	3.2 ± 0.5	90 ± 10	37 ± 2
R144K TcFIGase ^b	190 ± 20	160 ± 20	1200 ± 100
Mn ²⁺ -TcFIGase ^c	110 ± 20	50 ± 10	2300 ± 300
Co ²⁺ -TcFIGase ^c	50 ± 10	70 ± 20	800 ± 200
Ni ²⁺ -TcFIGase ^c	40 ± 10	90 ± 20	400 ± 100
Mg ²⁺ -TcFIGase ^c	90 ± 40	200 ± 60	400 ± 30

^aEnzyme expressed and purified from LB media. ^bEnzyme expressed and purified from minimal media supplemented with 100 μM MnCl₂ prior to induction. ^cEnzyme prepared by reconstituting the metal-free apoenzyme with divalent metal ions. ^dApparent K_M from Hill equation due to allosteric behavior.

metal ligands appear to be easily interchangeable in the metalloureohydrolase active site, as first demonstrated in structure–function studies of H101N rat arginase I.^{39,40,46}

Inspection of the TcFIGase active site reveals a single arginine residue, R144 (Figure 3a), that is strictly conserved among formiminoglutamase enzymes from different organisms (Figure 8). To investigate the possible function of this residue, the R144A, R144E, and R144K mutants were prepared and assayed (Table 3). Each mutant was expressed and purified from minimal media supplemented with MnCl₂ to exclude potential contamination by other metal ions. The sole incorporation of Mn²⁺ via this method was verified by ICP-AES analysis of the wild-type enzyme (Table 2). The R144A mutation causes a 38-fold reduction in catalytic efficiency, and the R144E mutation causes an even more severe 269-fold reduction in catalytic efficiency, relative to that measured for the wild-type enzyme. Notably, the R144K mutation retains near-normal catalytic efficiency (85% compared with the wild-type enzyme). These data suggest that the positively charged R144 side chain is critical for maximal catalysis.

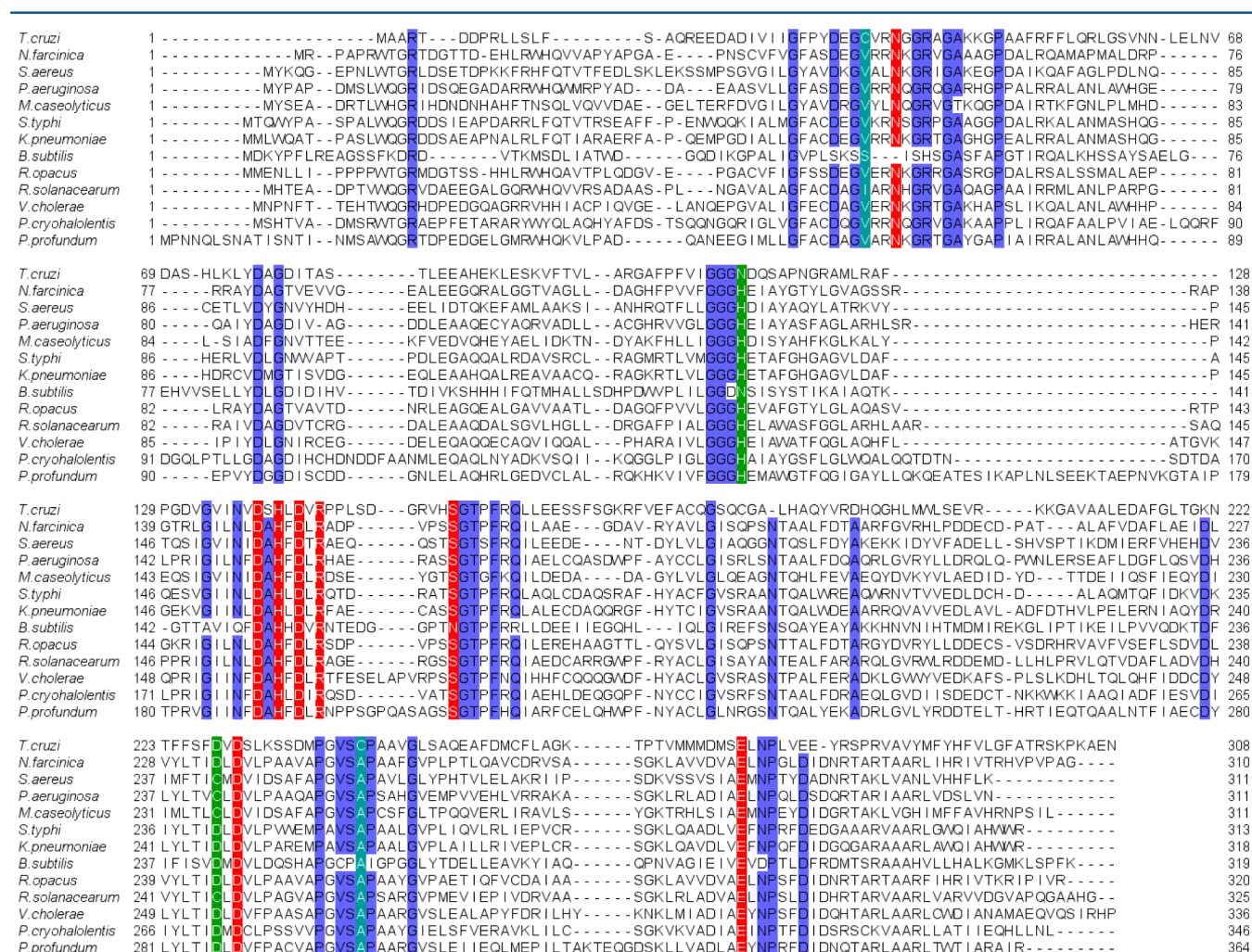


Figure 8. Sequence alignment of TcFIGase with FIGase enzymes identified in different bacteria. Sequences were aligned using Clustal Omega⁵² and displayed with Jalview.⁵³ Highly conserved active site residues (identity ≥90%) are highlighted in red. Moderately conserved active site residues (identity <90%) are highlighted in green. C35 and C242 (which can form a disulfide linkage in *T. cruzi*) and their equivalent residues in other species are highlighted in cyan. Other conserved residues (identity >90%) are highlighted in blue. Uniprot accession codes for aligned sequences are as follows: *Trypanosoma cruzi* (Q4DSA0), *Nocardia farcinica* (Q5ZOG1), *Macrococcus caseolyticus* (B9E7J8), *Pseudomonas aeruginosa* (Q9HZ59), *Staphylococcus aureus* (P99158), *Salmonella typhi* (Q8Z899), *Klebsiella pneumonia* (B5XZ82), *Bacillus subtilis* (P42068), *Rhodococcus opacus* (C1BBD1), *Ralstonia solanacearum* (Q8XW30), *Vibrio cholera* (Q9KSQ2), *Psychrobacter cryohalolentis* (Q1Q9E3), *Photobacterium profundum* (Q6LQ58).

Finally, to study the metal ion preference for catalysis by TcFIGase, apo-TcFIGase was reconstituted with different divalent metal ions and the catalytic activities of these metal-substituted enzymes were measured (Figure 9). ICP-

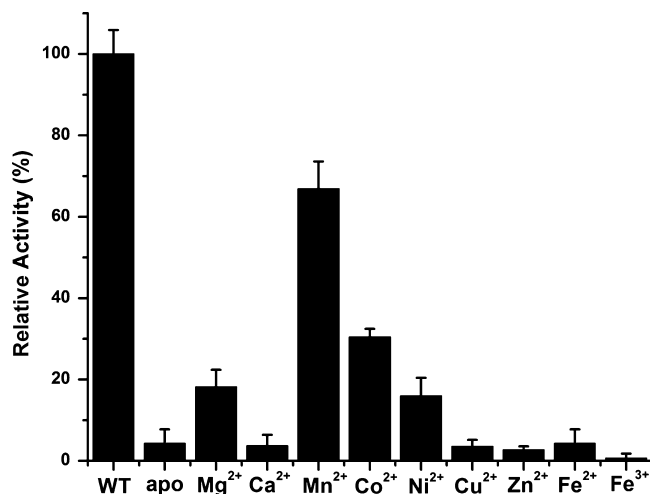


Figure 9. Dependence of TcFIGase activity on metal ions. Metal-free apoenzyme was prepared by depleting the metal ions at low pH using wild-type enzyme expressed and purified from LB media. Metal-substituted TcFIGase was reconstituted with 2 equivalents of metal ions and assayed for activity using 10 mM substrate. Activity was compared in terms of initial velocity.

AES measurements verified the preparation of apo-TcFIGase prior to reconstitution with different metal ions; equilibration of protein samples at low pH, and not treatment with metal ion chelators, successfully enabled metal ion dissociation. The apoenzyme retains 4% residual activity, which presumably results from a low concentration of residual Mn²⁺ ions contained in the protein sample as detected by ICP-AES (Table 2). The Mn²⁺-reconstituted enzyme exhibits 67% activity compared to the native wild-type enzyme. The inability to restore full activity by reconstituting the metal-free apoenzyme with Mn²⁺ suggests that the acidic pH treatment required to dissociate active site metal ions might cause some irreversible damage to the protein. This would be consistent with our observation that the apoenzyme is less stable than the metal-loaded enzyme and more susceptible to precipitation. However, in comparison with all other divalent metal ions tested, reconstitution of the apoenzyme with Mn²⁺ confers the highest level of catalytic activity. Therefore, Mn²⁺ is most likely to be the natural cofactor of TcFIGase. Furthermore, titration of metal-free TcFIGase with increasing concentrations of Mn²⁺ indicates that maximal activity requires the binding of more than one metal ion (Figure 10), suggesting that a binuclear manganese cluster is required for catalysis.

DISCUSSION

Metal Ion Function and Evolutionary Relationships.

The results outlined above demonstrate that TcFIGase is a manganese-dependent metallohydrolase, which is consistent with the essential catalytic role of Mn²⁺ in the ureohydrolase family of metalloenzymes as well as previous findings with formiminoglutamases from other species.^{21,22} The depletion of Mn²⁺ to yield apo-TcFIGase leads to a dramatic loss of activity, as shown in Figure 9. Catalytic activity is restored by the incubation of apo-TcFIGase with the divalent metal ions Mg²⁺, Mn²⁺, Co²⁺, and Ni²⁺, with maximal activity resulting from incubation with

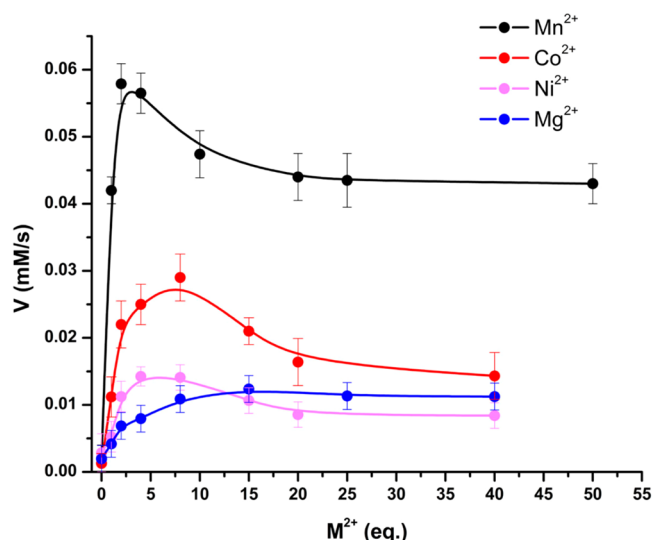


Figure 10. Dependence of TcFIGase catalysis on metal ion stoichiometry. Metal-free enzyme (20 μM) was incubated with increasing molar equivalents (eq) of divalent metal ions in assay buffer at 4 °C for 30 min. The reaction was initiated by addition of 1 mM substrate and monitored as described in the text. Maximal catalysis requires ≈2 Mn²⁺ ions per monomer.

Mn²⁺. However, in contrast with a binuclear manganese ureohydrolase such as arginase, in which a binuclear manganese cluster was first definitively demonstrated by electron paramagnetic resonance spectroscopy,⁴⁷ TcFIGase contains only 1 equivalent of Mn²⁺ bound tightly per monomer in solution as determined by ICP-AES (Table 2). Even so, maximal catalytic activity requires ≈2 Mn²⁺ ions bound per TcFIGase monomer (Figure 10). Furthermore, the X-ray crystal structure shows that both the A and B metal binding sites in TcFIGase are capable of binding Mn²⁺ ions when crystals of apo-TcFIGase are soaked in a buffer solution containing millimolar Mn²⁺ ion concentrations.

To account for the differences between ICP-AES measurements on the one hand, and Mn²⁺ titration studies and X-ray crystal structures on the other hand, we hypothesize that the Mn²⁺_B ion is more tightly bound and the Mn²⁺_A ion is more weakly bound. Resultantly, the Mn²⁺_A ion is more labile. This metal binding behavior is in accord with the observation that the Mn²⁺_B site is preferentially the first to be occupied when crystals of apo-TcFIGase are soaked in a Mn²⁺-containing buffer solution as the pH is gradually raised (data not shown); it is additionally in accord with crystal structures of Mn²⁺₂-TcFIGase_{ox} in which the Mn²⁺_B occupancy is always full, whereas the Mn²⁺_A occupancy is variable (Figure 7). This postulate is also consistent with ICP-AES measurements showing that 1 equivalent of Mn²⁺ remains bound per monomer after extensive dialysis and treatment with metal ion chelators. It is interesting to note that similar behavior is observed for metal ion binding to rat arginase I, from which only Mn²⁺_A can be extracted by treatment with metal ion chelators.³⁹ However, contrasting behavior is observed for arginase from *B. caldovelox*, from which the Mn²⁺_B ion is more weakly bound and preferentially removed by treatment with EDTA.⁴² In further contrast, both metal ions of human arginase I are readily removed by dialysis against DPA.³⁸

To investigate whether the weak binding of the Mn²⁺_A ion of Mn²⁺₂-TcFIGase is attributable to N114, N114H TcFIGase was prepared. This amino acid substitution restores an authentic arginase-like metal coordination polyhedron. Interestingly,

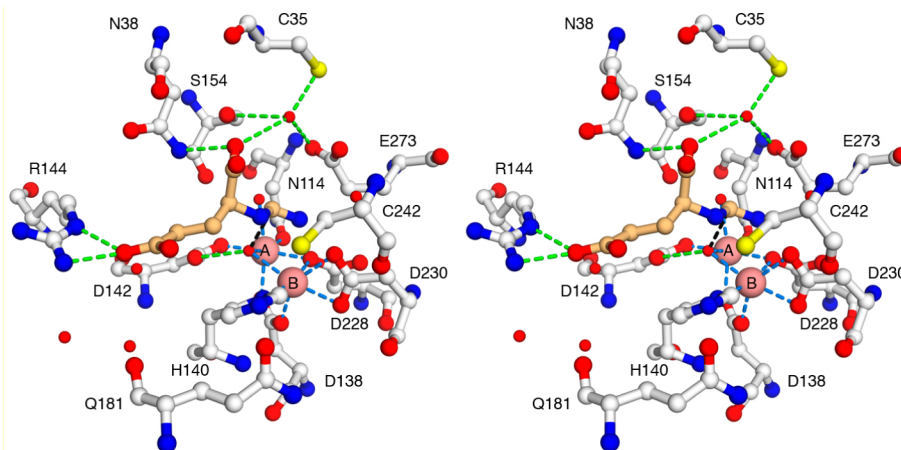


Figure 11. Hypothetical model of substrate binding in TcFIGase. One water molecule originally in the active site is deleted and the conformations of R144 and C242 are manually adjusted to accommodate the substrate. Metal coordination interactions are shown as blue dashed lines, and hydrogen bonds are indicated by green dashed lines. The Bürgi–Dunitz trajectory for nucleophilic attack by the metal-bridging hydroxide ion at the substrate imino group is indicated by a black dashed line.

Cavalli and colleagues⁴⁶ show that H101N rat arginase I exhibits 50% activity compared to wild-type rat arginase I; following dialysis, the metal–protein stoichiometry is measured to be 3.3 Mn^{2+} ions/trimer, suggesting weaker binding of the Mn^{2+}_A ion. Although this result might suggest that a histidine ligand is more favorable than an asparagine ligand to the Mn^{2+}_A ion, the N114H substitution in TcFIGase does not enhance Mn^{2+}_A affinity because protein–metal stoichiometry in the mutant is comparable to that of the wild-type enzyme (Table 2). In the crystalline mutant, too, the Mn^{2+}_B ion remains fully occupied whereas the Mn^{2+}_A ion is only partially occupied.

Amino acid sequence alignment of FIGase enzymes from different organisms suggests that the Mn^{2+}_A site is more variable than the Mn^{2+}_B site (Figure 8); specifically, the histidine ligand to Mn^{2+}_A is substituted by asparagine in the FIGase enzymes from *T. cruzi* and *B. subtilis*. Interestingly, the bridging aspartate ligand D228 of TcFIGase appears as cysteine in the FIGase enzymes from *S. aureus*, *P. aeruginosa*, *M. caseolyticus*, and *R. solanacearum*. The greater evolutionary potential of Mn^{2+}_A site ligands and weaker binding of Mn^{2+}_A is consistent with the fact that only the Mn^{2+}_B site is conserved among members of the greater arginase/deacetylase superfamily (the Mn^{2+}_B site of arginase-like enzymes such as TcFIGase corresponds to the Zn^{2+} site of histone deacetylases).^{19,48} The arginases and deacetylases share a common α/β fold and thus likely evolved from a common metallohydrolase ancestor.^{19,49} Therefore, FIGase, which shows notable variability in the Mn^{2+}_A binding site among the ureohydrolases, could represent a “snapshot” of an intermediate evolutionary state for the metal binding site between the arginases and the deacetylases.

Structural Insights on the Catalytic Mechanism. Despite the absence of a structure of TcFIGase complexed with a substrate or transition state analogue, important mechanistic inferences can be drawn from the structure of inactivated *B. caldovelox* arginase complexed with L-arginine⁴² and the structures of arginase from various organisms complexed with the boronic acid substrate analogue 2(S)-amino-6-borono-hexanoic acid.^{33–35,50} This analogue binds to arginase as the tetrahedral boronate anion, which mimics the tetrahedral intermediate and its flanking transition states in the arginase reaction. By analogy with ligand binding in the active site of arginase, we have modeled the binding of substrate L-formimino-

glutamate in the active site of Mn^{2+}_2 -TcFIGase (Figure 11). This model shows that four residues universally conserved among FIGase enzymes (Figure 8)—R144, N38, S154 and E273—could be involved in substrate binding. The negatively charged carboxylate side chain of E273 may play a role in substrate recognition by interacting with the positively charged iminium group of L-formiminoglutamate; the corresponding glutamate residue of arginase similarly interacts with the positively charged guanidinium group of L-arginine.^{42,50} The side chain of N38 is well-positioned to make a direct hydrogen bond with the α -carboxylate group of L-formiminoglutamate, and the side chains of S154, E273, and C35 may also make water-mediated hydrogen bonds with this α -carboxylate group, as shown in Figure 11. Finally, R144 is well-positioned to form a salt link with the side chain carboxylate group of L-formiminoglutamate. Indeed, the catalytic activities of R144A, R144E, and R144K TcFIGase indicate that a positive charge at this position is crucial for maximal catalysis (Table 3).

Since two solvent molecules are bound to the binuclear manganese cluster of TcFIGase, it could be questioned as to which of these solvent molecules is the catalytic nucleophile. However, the pK_a of a metal-bridging solvent molecule will be lower than that of a solvent molecule coordinated to just a single metal ion; therefore, a higher concentration of nucleophilic hydroxide ions would occupy a metal-bridging position compared with a single-metal coordination position. Also notable is the fact that as modeled in Figure 11, the lone electron pair of the presumed metal-bridging hydroxide ion is aligned with the Bürgi–Dunitz trajectory for nucleophilic attack at the π^* orbital of the substrate imino group. Interestingly, the model additionally suggests that the N δ atom of the formimino group would be oriented toward Mn^{2+}_B —perhaps implying that Mn^{2+}_A is not as important for transition state stabilization. This contrasts with the mechanistic proposal set forth for arginase, in which the N η 2 atom of L-arginine coordinates to Mn^{2+}_A as the tetrahedral intermediate is approached.⁴⁹

CONCLUSIONS

The results of the current study clearly demonstrate that the metal-free *T. cruzi* protein with undetermined function annotated as “arginase superfamily protein” by the Structural Genomics of Pathogenic Protozoa Consortium²⁰ (PDB entry

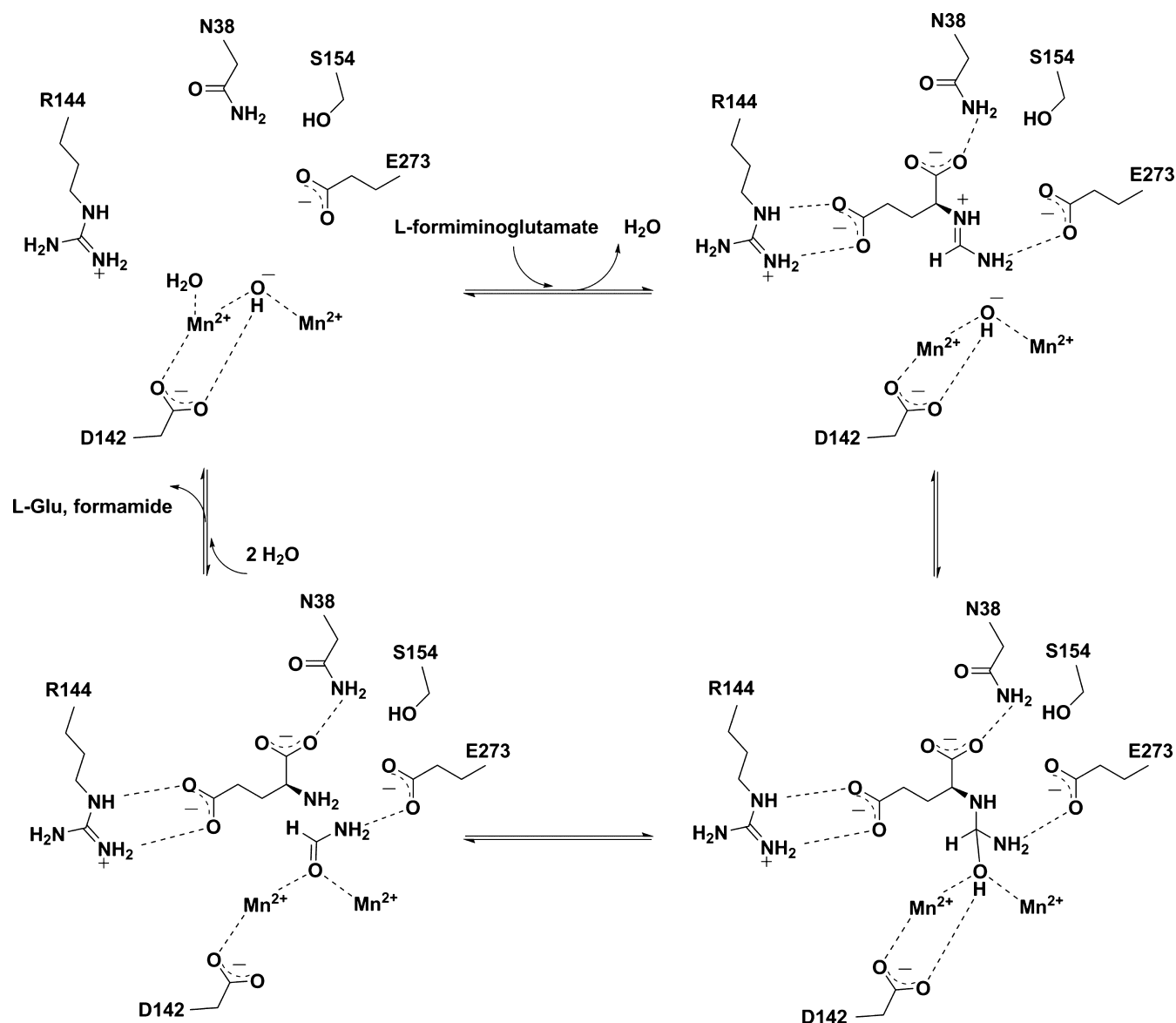


Figure 12. Proposed catalytic mechanism for Mn^{2+} -TcFIGase.

2A0M) is in fact a Mn^{2+} -dependent formiminoglutamase capable of binding a binuclear manganese cluster comparable to that first observed in rat arginase I.¹⁵ Mechanistic inferences emanating from structure–function studies of TcFIGase are summarized in the mechanistic proposal presented in Figure 12, in which the side chains of N38, R144, S154, and E273 function in substrate binding. We propose that TcFIGase utilized a metal-activated hydroxide mechanism for the hydrolysis of the substrate formimino group, which proceeds through a neutral tetrahedral intermediate stabilized by metal coordination as well as hydrogen bonds with D142 and E273. Proton transfer from the hydroxyl group to the leaving amino group of the tetrahedral intermediate facilitates collapse of the tetrahedral intermediate and product dissociation. In general, an amine must be protonated in order to be a leaving group in the collapse of a tetrahedral intermediate. Since D142 is close to both the metal-bridging hydroxide ion and the α -amino group of formiminoglutamate in the model of the enzyme–substrate complex shown in Figure 11, it is possible that D142 mediates this proton transfer – this would ensure that L-glutamate and not ammonia is the leaving group in the collapse of

the tetrahedral intermediate shown in Figure 12. There is no suitably oriented proton donor group that could enable the departure of ammonia based on the model of the enzyme–substrate complex (Figure 11), for example, as achieved by H269 in *N*-formimino-L-glutamate iminohydrolase; this enzyme adopts an unrelated fold and catalyzes the HutF reaction shown in Figure 1.^{45,51} The binding and ionization of additional solvent completes the catalytic cycle of TcFIGase. The synthesis and study of tetrahedral transition state analogues complexed with TcFIGase will allow us to test structural aspects of this mechanistic proposal, which we will report in due course.

■ ASSOCIATED CONTENT

Accession Codes

The atomic coordinates and structure factors have been deposited in the Protein Data Bank (www.rcsb.org) with accession codes 4MXR, 4MYN, 4MYL, 4MYF, and 4MYK, respectively.

AUTHOR INFORMATION

Corresponding Author

*E-mail: chris@sas.upenn.edu. Fax: (215) 573-2112. Tel: (215) 898-5714.

Present Address

[†]The Episcopal Academy, 1785 Bishop White Drive, Newtown Square, PA 19073

Funding

This work was supported by National Institutes of Health Grant GM49758.

Notes

The authors declare no competing financial interest.

ACKNOWLEDGMENTS

We thank Dr. Ethan Merritt for supplying the TcFIGase plasmid, and we thank the National Synchrotron Light Source at Brookhaven National Laboratory (beamline X29) for access to X-ray crystallographic data collection facilities. Additionally, we thank Dr. Kelley Bethony in the Science Department of the Episcopal Academy for helpful scientific discussions.

ABBREVIATIONS

TCEP, Tris(2-carboxyethyl)phosphine hydrochloride; BME, β -mercaptoethanol; TcFIGase, *Trypanosoma cruzi* formiminoglutamase; EDTA, ethylenediaminetetraacetic acid; DPA, dipicolinic acid; LB, lysogeny broth; PDB, Protein Data Bank; r.m.s., root-mean-square; ICP-AES, inductively coupled plasma-atomic emission spectrometry

REFERENCES

- Caspi, R., Altman, T., Dreher, K., Fulcher, C. A., Subhraveti, P., Keseler, I. M., Kothari, A., Krummenacker, M., Latendresse, M., Mueller, L. A., Ong, Q., Paley, S., Pujar, A., Shearer, A. G., Travers, M., Weerasinghe, D., Zhang, P., and Karp, P. D. (2012) The MetaCyc database of metabolic pathways and enzymes and the BioCyc collection of pathway/genome databases. *Nucleic Acids Res.* 40, D742–D753.
- Bender, D. A. (2012) *Amino Acid Metabolism*, pp 305–322, John Wiley and Sons, Ltd, Chichester, U.K.
- Hedegaard, J., Brevet, J., and Roche, J. (1966) Imidazole lactic acid: an intermediate in L-histidine degradation in *Escherichia coli* B. *Biochem. Biophys. Res. Commun.* 25, 335–339.
- Emes, A. V., and Hassall, H. (1973) Degradation of L-histidine in rat. The formation of imidazolylpyruvate, imidazolylactate and imidazolylpropionate. *Biochem. J.* 136, 649–658.
- Cortese, R., Brevet, J., and Hedegaard, J. (1968) Characterization of an imidazolepyruvic acid reducing system from *Escherichia coli* B. *Biochem. Biophys. Res. Commun.* 31, 209–215.
- Tabor, H., Mehler, A. H., Hayaishi, O., and White, J. (1952) Urocanic acid as an intermediate in the enzymatic conversion of histidine to glutamic and formic acids. *J. Biol. Chem.* 196, 121–128.
- Mehler, A. H., and Tabor, H. (1953) Deamination of histidine to form urocanic acid in liver. *J. Biol. Chem.* 201, 775–784.
- Miller, A., and Waelsch, H. (1957) Formimino transfer from formamidinoglutamic acid to tetrahydrofolic acid. *J. Biol. Chem.* 228, 397–417.
- Bender, R. A. (2012) Regulation of the histidine utilization (hut) system in bacteria. *Microbiol. Mol. Biol. Rev.* 76, 565–584.
- Brown, D. D., and Kies, M. W. (1959) The mammalian metabolism of L-histidine: I. The enzymatic formation of L-hydantoin-5-propionic acid. *J. Biol. Chem.* 234, 3182–3187.
- Hassall, H., and Greenberg, D. M. (1968) Studies on the enzymic decomposition of urocanic acid: VI. Properties of the enzyme catalyzing the oxidation of 4(5)-imidazolone-5(4)-propionic acid to L-hydantoin-5-propionic acid. *Arch. Biochem. Biophys.* 125, 278–285.

- Hassall, H., and Greenberg, D. M. (1963) The bacterial metabolism of L-hydantoin-5-propionic acid to carbamyl-glutamic acid and glutamic acid. *J. Biol. Chem.* 238, 3325–3329.
- Ouzounis, C. A., and Kyriakides, N. C. (1994) On the evolution of arginases and related enzymes. *J. Mol. Evol.* 39, 101–104.
- Perozich, J., Hempel, J., and Morris, S. M., Jr (1998) Roles of conserved residues in the arginase family. *Biochim. Biophys. Acta, Protein Struct. Mol. Enzymol.* 1382, 23–37.
- Kanyo, Z. F., Scolnick, L. R., Ash, D. E., and Christianson, D. W. (1996) Structure of a unique binuclear manganese cluster in arginase. *Nature* 383, 554–557.
- Elkins, J. M., Clifton, I. J., Hernandez, H., Doan, L. X., Robinson, C. V., Schofield, C. J., and Hewitson, K. S. (2002) Oligomeric structure of proclavaminic acid amidino hydrolase: evolution of a hydrolytic enzyme in clavulanic acid biosynthesis. *Biochem. J.* 366, 423–434.
- Ahn, H. J., Kim, K. H., Lee, J., Ha, J.-Y., Lee, H. H., Kim, D., Yoon, H.-J., Kwon, A.-R., and Suh, S. W. (2004) Crystal structure of agmatinase reveals structural conservation and inhibition mechanism of the ureohydrolase superfamily. *J. Biol. Chem.* 279, 50505–50513.
- Lee, S. J., Kim, D. J., Kim, H. S., Lee, B. I., Yoon, H.-J., Yoon, J. Y., Kim, K. H., Jang, J. Y., Im, H. N., An, D. R., Song, J.-S., Kim, H.-J., and Suh, S. W. (2011) Crystal structures of *Pseudomonas aeruginosa* guanidinobutyrase and guanidinopropionase, members of the ureohydrolase superfamily. *J. Struct. Biol.* 175, 329–338.
- Dowling, D. P., Costanzo, L., Gennadios, H. A., and Christianson, D. W. (2008) Evolution of the arginase fold and functional diversity. *Cell. Mol. Life Sci.* 65, 2039–2055.
- Fan, E., Baker, D., Fields, S., Gelb, M. H., Buckner, F. S., Van Voorhis, W. C., Phizicky, E., Dumont, M., Mehlin, C., Grayhack, E., Sullivan, M., Verlinde, C., DeTitta, G., Meldrum, D. R., Merritt, E. A., Earnest, T., Soltis, M., Zucker, F., Myler, P. J., Schoenfeld, L., Kim, D., Worthey, L., LaCount, D., Vignali, M., Li, J., Mondal, S., Massey, A., Carroll, B., Gulde, S., Luft, J., DeSoto, L., Holl, M., Caruthers, J., Bosch, J., Robien, M., Arakaki, T., Holmes, M., Le Trong, I., and Hol, W. G. J. (2008) in *Methods in Molecular Biology—Structural Proteomics: High-Throughput Methods*. (Kobe, B., Guss, M., and Huber, T., Eds.), Vol. 426, pp 497–513, Humana Press, Totowa, NJ.
- Lund, P., and Magasanik, B. (1965) N-formimino-L-glutamate formiminohydrolase of *Aerobacter aerogenes*. *J. Biol. Chem.* 240, 4316–4319.
- Kaminskas, E., Kimhi, Y., and Magasanik, B. (1970) Urocanase and N-formimino-L-glutamate formiminohydrolase of *Bacillus subtilis*, two enzymes of the histidine degradation pathway. *J. Biol. Chem.* 245, 3536–3544.
- Bradford, M. M. (1976) A rapid and sensitive method for the quantitation of microgram quantities of protein utilizing the principle of protein-dye binding. *Anal. Biochem.* 72, 248–254.
- Otwinowski, Z., and Mino, W. (1997) Processing of X-ray diffraction data collected in oscillation mode. *Methods Enzymol.* 276, 307–326.
- Adams, P. D., Afonine, P. V., Bunkóczi, G., Chen, V. B., Davis, I. W., Echols, N., Headd, J. J., Hung, L.-W., Kapral, G. J., Grosse-Kunstleve, R. W., McCoy, A. J., Moriarty, N. W., Oeffner, R., Read, R. J., Richardson, D. C., Richardson, J. S., Terwilliger, T. C., and Zwart, P. H. (2010) PHENIX: a comprehensive Python-based system for macromolecular structure solution. *Acta Crystallogr. D* 66, 213–221.
- McCoy, A. J., Grosse-Kunstleve, R. W., Storoni, L. C., and Read, R. J. (2005) Likelihood-enhanced fast translation functions. *Acta Crystallogr. D* 61, 458–464.
- Collaborative Computational Project, Number 4 (1994) The CCP4 suite: Programs for protein crystallography. *Acta Crystallogr. D* 50, 760–763.
- Emsley, P., Lohkamp, B., Scott, W. G., and Cowtan, K. (2010) Features and development of Coot. *Acta Crystallogr. D* 66, 486–501.
- Laskowski, R. A., MacArthur, M. W., Moss, D. S., and Thornton, J. M. (1993) PROCHECK: A program to check the stereochemical quality of protein structures. *J. Appl. Crystallogr.* 26, 283–291.

- (30) Kabsch, W., and Sander, C. (1983) Dictionary of protein secondary structure: pattern recognition of hydrogen-bonded and geometrical features. *Biopolymers* 22, 2577–2637.
- (31) Archibald, R. M. (1945) Colorimetric determination of urea. *J. Biol. Chem.* 157, 507–518.
- (32) Cama, E., Colleluori, D. M., Emig, F. A., Shin, H., Kim, S. W., Kim, N. N., Traish, A. M., Ash, D. E., and Christianson, D. W. (2003) Human arginase II: crystal structure and physiological role in male and female sexual arousal. *Biochemistry* 42, 8445–8451.
- (33) Di Costanzo, L., Sabio, G., Mora, A., Rodriguez, P. C., Ochoa, A. C., Centeno, F., and Christianson, D. W. (2005) Crystal structure of human arginase I at 1.29-Å resolution and exploration of inhibition in the immune response. *Proc. Natl. Acad. Sci. U.S.A.* 102, 13058–13063.
- (34) Dowling, D. P., Ilies, M., Olszewski, K. L., Portugal, S., Mota, M. M., Llinás, M., and Christianson, D. W. (2010) Crystal structure of arginase from *Plasmodium falciparum* and implications for L-arginine depletion in malarial infection. *Biochemistry* 49, 5600–5608.
- (35) D'Antonio, E. L., Ullman, B., Roberts, S. C., Dixit, U. G., Wilson, M. E., Hai, Y., and Christianson, D. W. (2013) Crystal structure of arginase from *Leishmania mexicana* and implications for the inhibition of polyamine biosynthesis in parasitic infections. *Arch. Biochem. Biophys.* 535, 163–176.
- (36) Krissinel, E., and Henrick, K. (2007) Inference of macromolecular assemblies from crystalline state. *J. Mol. Biol.* 372, 774–797.
- (37) Delano, W. D. (2007) *MacPyMol: A PyMol-based molecular graphics application for MacOS X*, DeLano Scientific LLC, Palo Alto, CA.
- (38) D'Antonio, E. L., and Christianson, D. W. (2011) Crystal structures of complexes with cobalt-reconstituted human arginase I. *Biochemistry* 50, 8018–8027.
- (39) Scolnick, L. R., Kanyo, Z. F., Cavalli, R. C., Ash, D. E., and Christianson, D. W. (1997) Altering the binuclear manganese cluster of arginase diminishes thermostability and catalytic function. *Biochemistry* 36, 10558–10565.
- (40) Cama, E., Emig, F. A., Ash, D. E., and Christianson, D. W. (2003) Structural and functional importance of first-shell metal ligands in the binuclear manganese cluster of arginase I. *Biochemistry* 42, 7748–7758.
- (41) Di Costanzo, L., Pique, M. E., and Christianson, D. W. (2007) Crystal structure of human arginase I complexed with thiosemicarbazide reveals an unusual thiocarbonyl μ -sulfide ligand in the binuclear manganese cluster. *J. Am. Chem. Soc.* 129, 6388–6389.
- (42) Bewley, M. C., Jeffrey, P. D., Patchett, M. L., Kanyo, Z. F., and Baker, E. N. (1999) Crystal structures of *Bacillus caldovelox* arginase in complex with substrate and inhibitors reveal new insights into activation, inhibition and catalysis in the arginase superfamily. *Structure* 7, 435–448.
- (43) Petřek, M., Košinová, P., Koča, J., and Otyepka, M. (2007) MOLE: a Voronoi diagram-based explorer of molecular channels, pores, and tunnels. *Structure* 15, 1357–1363.
- (44) Schmidt, B., Ho, L., and Hogg, P. J. (2006) Allosteric disulfide bonds. *Biochemistry* 45, 7429–7433.
- (45) Martí-Arbona, R., Xu, C., Steele, S., Weeks, A., Kutý, G. F., Seibert, C. M., and Raushel, F. M. (2006) Annotating enzymes of unknown function: N-formimino-L-glutamate deiminase is a member of the amidohydrolase superfamily. *Biochemistry* 45, 1997–2005.
- (46) Cavalli, R. C., Burke, C. J., Soprano, D. R., Kawamoto, S., and Ash, D. E. (1994) Mutagenesis of rat liver arginase expressed in *Escherichia coli*: role of conserved histidines. *Biochemistry* 33, 10652–10657.
- (47) Reczkowski, R. S., and Ash, D. E. (1992) EPR evidence for binuclear manganese(II) centers in rat liver arginase. *J. Am. Chem. Soc.* 114, 10992–10994.
- (48) Lombardi, P. M., Cole, K. E., Dowling, D. P., and Christianson, D. W. (2011) Structure, mechanism, and inhibition of histone deacetylases and related metalloenzymes. *Curr. Opin. Struct. Biol.* 21, 735–743.
- (49) Christianson, D. W. (2005) Arginase: structure, mechanism, and physiological role in male and female sexual arousal. *Acc. Chem. Res.* 38, 191–201.
- (50) Cox, J. D., Kim, N. N., Traish, A. M., and Christianson, D. W. (1999) Arginase-boronic acid complex highlights a physiological role in erectile function. *Nat. Struct. Biol.* 6, 1043–1047.
- (51) Martí-Arbona, R., and Raushel, F. M. (2006) Mechanistic characterization of N-formimino-L-glutamate iminohydrolase from *Pseudomonas aeruginosa*. *Biochemistry* 45, 14256–14262.
- (52) Sievers, F., Wilm, A., Dineen, D., Gibson, T. J., Karplus, K., Li, W., Lopez, R., McWilliam, H., Remmert, M., Soding, J., Thompson, J. D., and Higgins, D. G. (2011) Fast, scalable generation of high-quality protein multiple sequence alignments using Clustal Omega. *Mol. Syst. Biol.* 7, 539.
- (53) Troshin, P. V., Procter, J. B., and Barton, G. J. (2011) Java bioinformatics analysis web services for multiple sequence alignment—JABAWS:MSA. *Bioinformatics* 27, 2001–2002.